2010

THEORETICAL MODELING AND ANALYSIS OF AMMONIA GAS SENSING PROPERTIES OF VERTICALLY ALIGNED MULTIWALLED CARBON NANOTUBE RESISTIVE SENSORS AND ENHANCING THEIR SENSITIVITY

Shripriya Darshini Poduri
University of Kentucky, shripriya.engg@gmail.com

ABSTRACT OF THESIS

THEORETICAL MODELING AND ANALYSIS OF AMMONIA GAS SENSING PROPERTIES OF VERTICALLY ALIGNED MWCNTS RESISTIVE SENSOR AND ENHANCING THEIR SENSITIVITY

Abstract: Vertically aligned Multiwalled Carbon Nanotubes (MWCNTs) were grown in the pores of Anodized Aluminum Oxide (AAO) templates and investigated for resistive sensor applications. High Sensitivity of 23% to low concentration (100 ppm) of ammonia was observed. An equivalent circuit model was developed to understand the current flow path in the resistive sensor. This helped us in achieving high sensitivities through amorphous carbon (a-C) layer thickness tailoring by employing post-growth processing techniques like plasma etching.

A simulation model in MATLAB was developed to calculate the device resistance and the change in the sensitivity as a function of device parameters. The steady state response and transient response of the model to the number of ammonia molecules and its adsorption rate were studied. Effects of oxygen plasma, argon plasma and water plasma etch on thinning of the a-C layer were studied.

In order to enhance the sensitivity, the top and bottom a-C layers were replaced by a more conductive metal layer. This also helped in understanding the current flow in the device and in the estimation of the resistivity of the a-C layer.

Keywords: Anodized Aluminum Oxide (AAO), Multiwall Carbon Nanotube (MWCNTs), Plasma Enhanced Chemical Vapor Deposition (PECVD), sensors.

Shripriya Darshini Poduri

July 26, 2010

THEORETICAL MODELING AND ANALYSIS OF AMMONIA GAS SENSING PROPERTIES OF VERTICALLY ALIGNED MWCNTS RESISTIVE SENSORS AND ENHANCING THEIR SENSITIVITY

By Shripriya Darshini Poduri

Director of Thesis:
Dr .Vijay Singh

Director of Graduate Studies
Dr. Stephen Gedney

RULES FOR THE USE OF THESIS

Unpublished theses submitted for the Master's degree and deposited in the University of Kentucky Library are as a rule open for inspection, but are to be used only with due regard to the rights of the authors. Bibliographical references may be noted, but quotations or summaries of parts may be published only with the permission of the author, and with the usual scholarly acknowledgments.

Extensive copying or publication of the thesis in whole or in part also requires the consent of the Dean of the Graduate School of the University of Kentucky.

A library that borrows this thesis for use by its patrons is expected to secure the signature of each user.

Name	**Date**

THESIS

Shripriya Darshini Poduri

The Graduate School
University of Kentucky
2010

THEORETICAL MODELING AND ANALYSIS OF AMMONIA GAS SENSING PROPERTIES OF VERTICALLY ALIGNED MULTIWALLED CARBON NANOTUBE RESISTIVE SENSORS AND ENHANCING THEIR SENSITIVITY

THESIS

A thesis submitted in partial fulfillment of the
requirements for the degree of Master of Science in
Electrical Engineering in the
College of Engineering
at the University of Kentucky

By
Shripriya Darshini Poduri
Lexington, Kentucky
Director: Dr. Vijay Singh Professor of Electrical and Computer Engineering
Lexington, Kentucky
2010

Acknowledgments

No research is ever the outcome of individual's efforts. This work presented in the thesis would not have been possible without the helping hands of others.

First of all, I would like to thank my advisor, Dr. Vijay Singh for giving me the opportunity and motivation to work with the theoretical modeling and developing a simulation model of the CNT based resistive sensor.

I am very grateful to Dr. Suresh Rajaputra for his excellent guidance and support throughout my thesis. He helped me and gave his excellent ideas about the experiments. I am very thankful to him for his guidance ideas to do research. I have learnt a lot from him about professional excellence and ways to do manage many tasks at a time. I would sincerely thank him a lot for his guidance and advice.

This thesis would have not been complete without the committee. I thank Dr. Vijay Singh, Dr. Zhi Chen and Dr. Todd Hastings for serving their time to read my thesis.

I would take this opportunity to thank Raghu Mangu for motivating me and giving me his valuable time and ideas. I am grateful to him for helping me whenever I had any problem. He helped me with many of my experiments.

I would also like to thank Dr.Chuck May, Brian Wajdyk for training me and making me familiar with the equipments at CENSE, University of Kentucky.

I would also take this opportunity to thank all my friends Swethasree Nimmagadda, Srikanth Durgahmohanty, Bhavnandan Reddy, Piao, Harsha Moturu and Sai Reddy for providing me a healthy, and friendly environment.

My family members deserve special thanks for their help and endless support. I would like to thank my father and mother for their support and blessings. Their support and blessings enabled me to stand confidently against all difficult times. I would also like to thank my sisters Aruna, Seetha and brother in- law Amit Khanna for their love, care and support.

Shripriya Poduri
Summer 2010

Contents

List of Figures

List of Tables

List of Equations

Chapter 1 Introduction

1.1 Introduction

Ever since their discovery by Iijima [1], a great deal of interest in carbon nanotube (CNTs) has been generated for various applications such as field emission devices [2], sensors and actuators [3],[4] and random access memory [5], etc. Recent applications of carbon nanotubes as gas sensors have been reported. Due to their large surface areas and because of their hollow center, they show excellent sensitivity, rapid response and recovery times. Gas sensors are used in many industrial, medical, and commercial applications. For example, ammonia sensors are used for monitoring ambient ammonia concentration since it is related to many environmental issues such as human health, acidification, and change in climate through particle formation [6].

Gas sensors based on CNTs mostly rely on monitoring the direct change in their electrical properties in response to the interaction with gaseous molecules [7–11]. When electron withdrawing molecules (e.g., NO_2 and O_2) are adsorbed on the surface of p-type semiconductor CNTs, the Fermi levels are shifted to the valence band, generating more holes and thus enhancing the conductance. The adsorption of electron-donating molecules (e.g., NH_3) causes the number of holes to decrease and the resistance to increase. The chemiresistor gas response is attributed to the *p*-type conductivity in semiconducting MWCNTs and the electrical charge transfer was found to be the major sensing mechanism responsible for the change in electrical properties. Therefore, networks of different carbon nanotube (CNT) materials were investigated as resistive gas sensors. The results obtained from the research demonstrate that the MWCNT-based

sensors exhibit high gas sensitivity, fast response and reversibility, good repeatability and reproducibility. Therefore, making good contacts between electrodes and CNTs with clean surfaces is essential for fabricating a good sensor.

In comparison to solid state sensors and SWCNT/MWCNT sensors, it was found that solid-state sensors for gases like NO_2 and NH_3 operate at temperatures more than 700 K, while SWCNT/MWCNT sensors usually operate at room temperature and have lower response times of about 10 seconds [12–15].This is an advantage over metal-oxide sensors [12, 15], which operate at high temperatures and require a heater to maintain higher temperatures, thereby making the design of the sensor complicated and costlier. On the other hand, polymer sensors have poor sensitivities and slower (10 min) response times [14]. It was observed that the response times of nanotube sensors were lower than those of solid-state sensors [12-15].

We used Multiwalled Carbon Nanotubes (MWCNTs) grown in Anodized Aluminum Oxide (AAO) templates as sensors which have a better response and recovery time, higher sensitivity, and operate at room temperature. It forms arrays of nano pores of uniform diameter and length, as the CNTs synthesized on the surface of the nano pore wall take the shape of the geometry of the nano pores in the AAO, thus forming regular arrays of nanotube of uniform diameter and length. The size of the nano pores in AAO is easily reproducible in anodization during its preparation. This ability to integrate into a uniform stable structure is very important in all the device fabrication procedures. Another important feature of this sensor device is that it is a vertical structure, which is not parallel to the surface structure in which it monitors the gases diffused into the nano pores and adsorbed on the inside wall of the CNTs. Therefore, we tested this structure as

a sensor by measuring the resistance change upon the gas adsorption in this study.

The main objective of this study is to develop a resistive gas sensor structure for mass production with an array of carbon nanotube synthesized on an anodic aluminum oxide (AAO) template. This device gives uniform performance due to the regular and uniform nano-channels in the AAO. It is a vertical structure having open-ended multi-wall carbon nanotube grown through CVD on the inside walls of the AAO, such that the gas would diffuse into the nano channels for adsorption. The results discussed in this thesis show that the sensor has high sensitivity of around 20 % after plasma etching the amorphous carbon layer by various techniques like microwave plasma oxidation in oxygen and argon [16].

Sputtering is basically a Physical Vapor deposition (PVD) of thin films which erodes the material from the target (source) and then deposits it on the wafer in an inert gas atmosphere, such as argon. Sputtered atoms ejected from the target are accelerated by the energetic inert gas ions impact on the substrates or vacuum chamber with full energy. They are deposited on the substrate or collided with the inert gas ions or diffused slowly on to the substrate and on walls of the chamber. Chemical reactions can also occur sometimes on the target surface, in-flight or on the substrate depending on the process parameters which make the sputter deposition a complex process, but can be very helpful in depositing very thin films on the substrate with much control.

In Plasma Enhanced Chemical Vapor deposition, the substrate was exposed to volatile precursors which chemically react or decompose on the substrate's surface, which in turn was enhanced by plasma. It had the advantages of flexibility with film properties, versatility to deposit any element or compound and high purity. The sensitivity can also

be enhanced by controlling the diameter and number of carbon nanotube or size of the sample which can be done by varying the interspacing of carbon nanotube and pore radius of the sample by changing the anodization conditions. [17-18].This also gives a faster response time of less than 1 min and good reproducible recovery behaviors in atmospheric pressure at room temperature.

1.2 Background

Recently, carbon nanotubes have been used as gas sensors due to their large surface area, which give them excellent sensitivity. Also, their response times and recovery times are fast. They show a remarkable change in electrical properties like resistance and capacitance upon exposure to reducing gases and oxidizing gases. Single Walled Carbon Nanotube (SWCNTs) has yielded the highest sensitivity of 22% change in resistance to the SWCNT-PABS composite sensor when they were exposed to 100 ppm ammonia [17]. Another SWCNT device had an initial 30% increase in resistance on exposure to 1% (1000 ppm) NH_3 after 1000 seconds [18]. The highest sensitivity of the aligned MWCNT sensor is 12% for the first pulse of gas and 5% in steady state [19, 20].

However, commercial solid state sensors operate at high temperatures more than 700 K due to which it requires a complicated and costly device involving a heater. Therefore, MWCNTs sensors were grown in the porous Anodized Alumina templates which are easy to prepare as no purification, or separation steps of the CNT's are required. Porous Alumina templates were having the best attributes for growing uniform pores of nanowires or nanotubes having high aspect ratio. Therefore, AAO was the best template for growing MWCNTs. It was also durable and could withstand high temperatures (up to 800 or 1000 ° C) [22], [25]. The length and diameter of the pores could also be controlled

by changing the experimental conditions [23], [24], [25], [26].This MWCNT aligned sensor usually offers reduced cost of production and yields a high sensitivity, good reproducibility, and best response and recovery times.

1.3 Description of the device

The MWCNTs are embedded in the pores of a porous alumina template. Electrical contact between tubes is provided by top and bottom conducting layers (amorphous carbon in as-grown sensors). Bus bars are placed along the sensor to measure the change resistance across them when exposed to detectable gas analytes.

These MWCNTs were grown in the pores of the Anodized Alumina template by Chemical Vapor Deposition (CVD).This template was about 60 μm thick and pores are of about 40 nm in diameter. The grown MWCNT in the template had a wall thickness of 10 nm and were open at both ends. Additionally, amorphous carbon (a-C), a byproduct of the CVD growth process, coated the top and bottom of the AAO/CNT template. Electrical contact between tubes was provided by top and bottom conducting layers (amorphous carbon in as-grown sensors). Bus bars were placed along the sensor to measure the resistance across them. When bus bar contacts were placed at both the ends of the top surface, the resistance between these contacts changed accordingly to oxidizing (resistance decreases) and reducing agents (resistance increases). The primary objective of the resistive sensor model was to understand the device resistance dependence upon the MWCNT resistance and the thickness of amorphous carbon, and the sensitivity dependence upon the device structure and design. With this understanding, the model offered avenues for device improvement.

1.4 Objectives and Contributions

The following is the list of objectives and contributions of this thesis:

- The change in device sensitivity and resistance with respect to a-C layer thickness was extensively studied. The higher the thickness of amorphous carbon, the lower the sensitivity.
- Theoretical modeling of the sensor design was proposed and the device resistance was calculated and compared with the actual resistance value.
- Another model was also developed to study the transient response of the device to ammonia gas molecules.
- A program was designed in MATLAB to calculate the resistance of the device.
- Various plasma etching techniques like plasma oxidation in microwave and PECVD chamber (Plasma Enhanced Chemical Vapor Deposition) were performed in order to remove amorphous carbon to improve the sensitivities.
- Water plasma was employed to remove the amorphous carbon in order to improve the sensitivity.
- After the removal of a-C layer, the top and bottom layers were sputtered with a more conductive metal layer to understand the relation of current flow paths with the sensitivity.

1.5 Outline of the thesis

Chapter 2.1 will give a brief introduction to carbon nanotube and its advantages for

being used as a sensor and other applications. Chapter 2.2 will give a detailed description of the theoretical model of the resistive sensor. A detailed MATLAB program to calculate the device resistance is composed. Theoretical model with the simulation results are all discussed in Chapter 2 and a model for the sensor response to the ammonia molecules and how it changes with respect to sensitivity and the number of electrons donated by test gas molecules and the acceptor density. Chapter 3 will explain about all the experimental procedures used to prepare the resistive sensor model. Chapter 3.1 will describe about the anodization of the template and then MWCNTs grown in the template by Chemical Vapor Deposition (CVD) will be discussed in detail in 3.2.The basic sensor system device used in sensing of the gas analytes and the process of removal of amorphous carbon to improve the sensitivity like microwave plasma oxidation and Plasma Enhanced Chemical Vapor Deposition (PECVD) etch is discussed in 3.3,3,4 and 3.5 respectively. Chapter 4 will discuss the results obtained after sensing. Results obtained by microwave plasma oxidation and PECVD are discussed in 4.1 and 4.2 respectively.4.3 will discuss about the results obtained for cycling data with water plasma and PECVD, and comparison of all these processes are discussed. Simulation results obtained from the MATLAB program are discussed. Variation of device resistance and resistance of top and bottom layer of a-C layer is discussed in detail. Chapter 5 will give the conclusion of the thesis work and provide directions for the future work.

Chapter 2: The theoretical model

2.1 Description of the model

The resistive sensor was prepared by growing MWCNTs by Chemical Vapor Deposition (CVD) in the pores of anodized alumina template as shown in Figure 2.1.The bus bars were placed to make electrical contacts by depositing colloidal graphite paste first and then the silver or gold paste was deposited over it in order to measure the electrical properties such as the resistance. A layer of amorphous carbon was formed on top and bottom sides, as a byproduct of the CVD process, which acted as a conducting layer and connected the MWCNTs electrically as shown in Figure 2.2 in the equivalent circuit model.

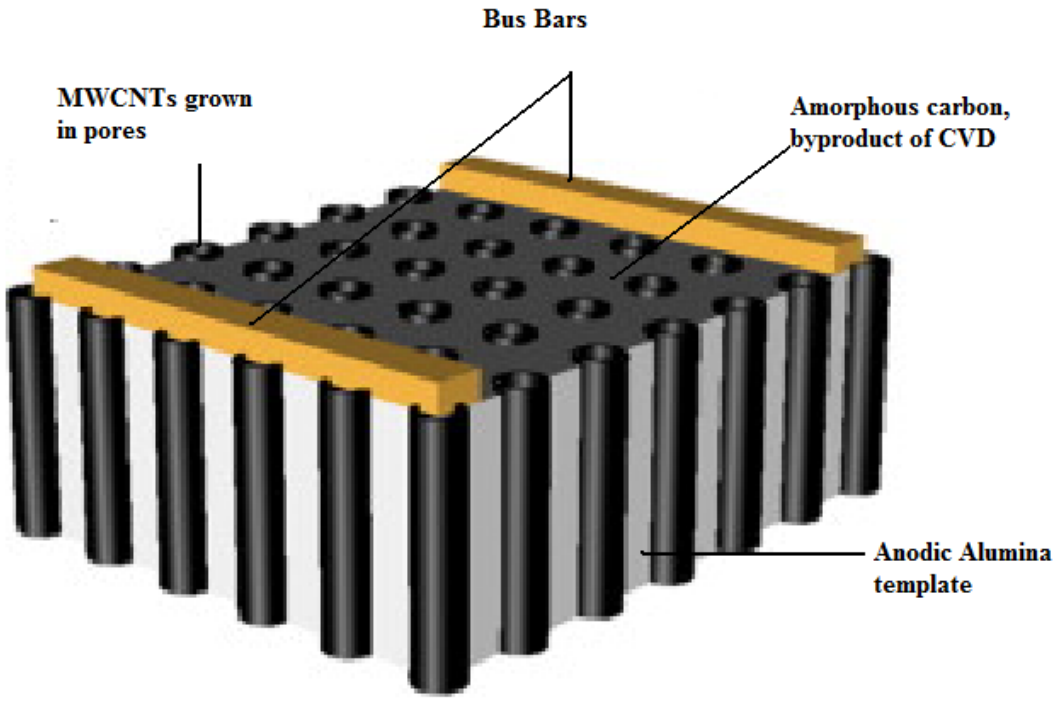

Figure 2.1: The resistive sensor model [66].

2.2 The operating principle

The sensor gas response was due to the *p*-type conductivity in semiconducting MWCNTs and the electrical charge transfer was found to be the major operating principle responsible for the change in electrical properties [21]. These gas sensors based on CNTs mostly rely on monitoring the direct change in their electrical properties in response to the interaction with gaseous molecules [7–11]. When electron withdrawing molecules of gas analytes (e.g., NO_2 and O_2) were adsorbed on the surface of p-type semiconductor CNTs, the Fermi levels were shifted to the valence band, generating more holes, thus enhancing the conductance. The adsorption of electron-donating molecules (e.g., NH_3) caused the number of holes to decrease and the resistance to increase whereas the adsorption of the electron withdrawing molecules (e.g. NO_2 gas) decreased the resistance of the sensor by generating more holes and shifting the Fermi Level towards the valence band.

The operating principle allowed us to design the model and suggested ways to improve its sensitivity by allowing the maximum current to flow through the MWCNTs.

The device can be considered as having two current paths (as shown in Figure 2.2):

- Direct current path from contact to another contact through the layer of conducting amorphous carbon (a-C)
- Other alternate path through the MWCNTs and the bottom conducting path.

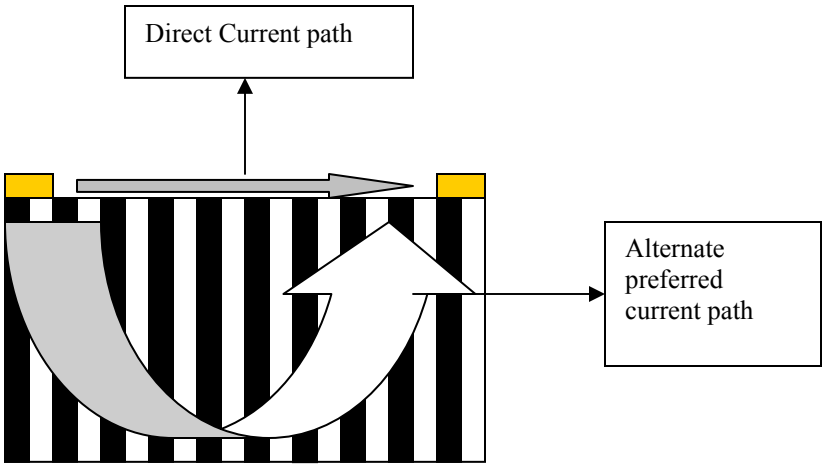

Figure 2.2: Resistive sensor model showing the 2 current flow paths: Direct current path between the bus bars through the top conducting amorphous carbon layer and the alternate preferred path through MWCNTs and bottom conducting amorphous carbon layer [70].

The direct path consisted of only the a-C layer without involving the CNTs, therefore it did not contribute to the sensitivity of the sensor model. The current should flow through the alternate path involving the MWCNTs and bottom conducting path of amorphous carbon layer, thus enhancing the sensitivity of the device. We needed to design the device in such a way that the sensitivity of the device was highest by allowing the current to flow through the alternate path. This could be done by changing the resistance of the top and bottom layer of amorphous carbon accordingly.

This could be done only if the theoretical model and its equivalent circuit of the sensor design are understood. Hence, we designed the theoretical model for the vertically aligned MWCNTs resistive sensor.

2.3 The equivalent circuit model for resistive sensor model

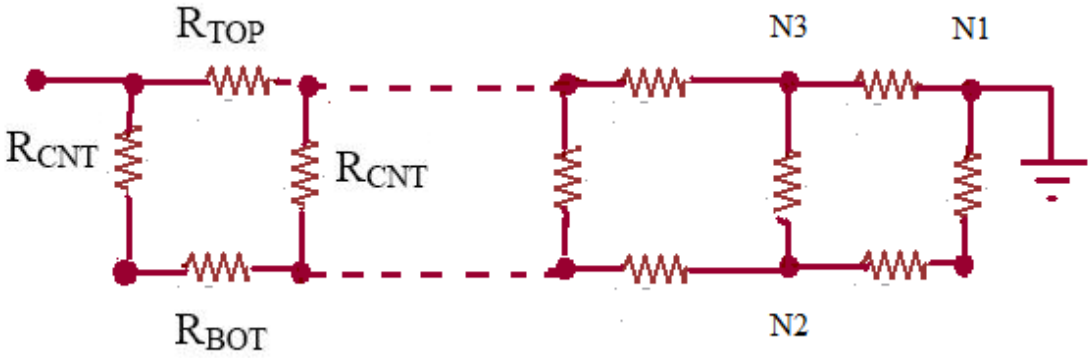

Figure 2.3: Equivalent circuit model showing R_{TOP}, R_{CNT}, and R_{BOT} of one row of 3D regular network of the device. Nodes N_1, N_2 and N_3 are shown as the nodes of the first Δ to Y transformation.

The equivalent circuit model is a regular 3D network of 3 resistances:

- Resistance of the top layer of amorphous carbon (R_{top}),
- Resistance of the MWCNT (R_{CNT}), and
- Resistance of the bottom layer of amorphous carbon (R_{bot}).

This equivalent circuit was developed to understand the operation of the sensor device and to find ways to improve the sensitivity of the device. The equivalent circuit shown in Figure 2.3 is of one row of vertically aligned MWCNT.

2.4 Equivalent row resistance

The equivalent row resistance is calculated by successive Δ-Y transformations along the row.

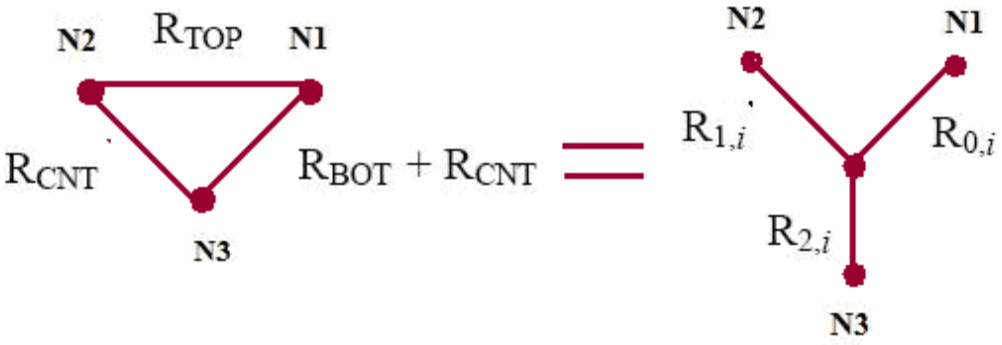

Figure 2.4: The nodes and label for each resistor for the first delta-wye transformation.

The resistance values after the first delta -wye transformation is given by the following equations:

$$R_{0,i} = \frac{R_{TOP}\,(R_{BOT} + R_{CNT})}{(2R_{CNT} + R_{TOP} + R_{BOT})} \qquad (2.1)$$

$$R_{1,i} = \frac{R_{CNT}R_{TOP}}{(2R_{CNT} + R_{TOP} + R_{BOT})} \qquad (2.2)$$

$$R_{2,i} = \frac{R_{CNT}\,(R_{BOT} + R_{CNT})}{(2R_{CNT} + R_{TOP} + R_{BOT})} \qquad (2.3)$$

N_1', N_2', and N_3' are the nodes after the second Δ-Y transformation in Figure 2.4.

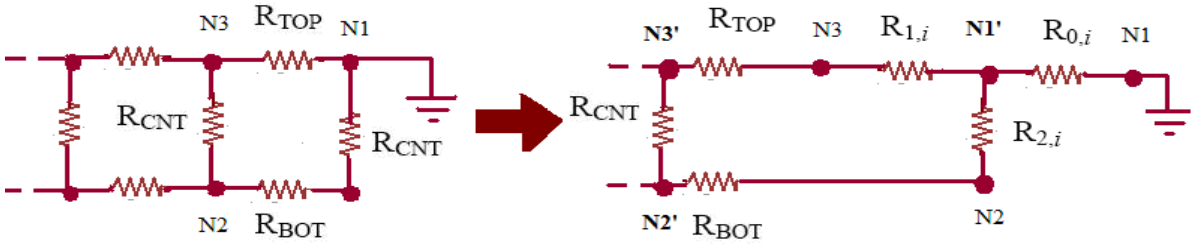

Figure 2.5: Schematic figure showing the label for nodes and resistances after the second delta to wye transformation.

The full equation for equivalent row resistance is given by (2.4). It is the sum of all $R_{0,i}$ terms starting from 1 to x, where x is the number of MWCNT's in the row. The first term,

$R_{0,1}$ is the initial first Δ to Y transformation. The second term is a summation of all $R_{0,i}$ terms from each transformation. The $R_{0,i}$ terms differ from $R_{0,1}$ because they depend on the $R_{1,i-1}$ $R_{2,i-1}$ terms from the previous transformation. The third term is the parallel resistance of two remaining resistances at the end of the row

$$R_{Row} = \sum_{i=1}^{x} R_{0,i} = \frac{R_{TOP}\,(R_{BOT} + R_{CNT})}{(2R_{CNT} + R_{TOP} + R_{BOT})} + \sum_{i=2}^{x-3} \frac{(R_{TOP} + R_{1,i})(R_{BOT} + R_{2,i})}{(R_{CNT} + (R_{TOP} + R_{1,i}) + (R_{BOT} + R_{2,i})}$$

$$+ \frac{(R_{TOP} + R_{1,x})(R_{CNT} + R_{BOT} + R_{2,x})}{(R_{CNT} + (R_{TOP} + R_{1,i}) + (R_{BOT} + R_{2,i}))} \qquad (2.4)$$

where the values for $R_{1,i,}$ and $R_{2,i}$ are given by [70] (2.5):

$$R_{(1,2),i} = \frac{R_{CNT}\,(R_{(TOP,BOT)} + R_{(1,2),i-1})}{(R_{CNT} + R_{(1,i-1)} + R_{(2,i-1)})}\,. \qquad (2.5)$$

Since the row resistance given by (2.4) is for one row of vertically aligned MWCNT Therefore, the device resistance is given by [70] (2.6),

$$1/R_{Device} = \sum_{i=1}^{y} \frac{1}{R_{Row}} \qquad (2.6)$$

where y is the number of rows of MWCNTs in y direction.

2.5 Layer of amorphous carbon and its top and bottom resistances RTOP and RBOT

The top and bottom layer amorphous carbon resistances, R_{TOP} and R_{BOT}, were calculated by using the resistivity formula

$$R = \frac{(\rho_{ac} \text{ x } L)}{A}\,.$$

Length L and Area A were calculated taking into consideration that the amorphous carbon does not cover the open pores as shown in Figure 2.6 [70].

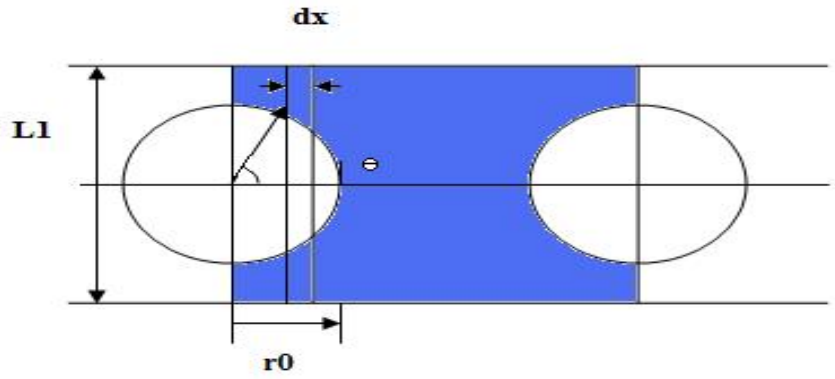

Figure 2.6 Figure shows the shaded area as the conducting path layer of amorphous carbon between adjacent MWCNT's.

L1 is the pore pitch in x and y directions, ro is the pore radius. θ is the angle from the x-axis inside the pore used in (2.7).

$$R_{(TOP,BOT)} = 2\left(\frac{\rho_{ac}}{2t_{acTOP,BOT}} \int_{\Theta=0}^{\Theta=pi/2} \frac{ro\ \sin\Theta d\Theta}{L1/2 - ro\sin\Theta} + \frac{\rho_{ac} \times (L1/2ro)}{(t_{acTOP,BOT} \times L1)}\right) . \quad (2.7)$$

For the standard templates used for experiments L1=85 nm and ro =20 nm.

Substituting these values of L1 and r0 in (2.7) the expression reduces [70] to

$$R_{(TOP,BOT)} = \frac{\rho_{ac}\ x1.29}{t_{acTOP,BOT}} . \quad (2.8)$$

2.6 Resistance of MWCNT

The resistance of the carbon nanotube was calculated [70] by:

$$R_{CNT} = \frac{4 \times \rho_{CNT}\ x\ h_{CNT}}{\Pi x(do^2 - di^2)} . \quad (2.9)$$

2.7 Image characterization to calculate pore density and other device parameters

We needed to read the SEM images of the samples to calculate the pore density/number of MWCNTs per unit length Nx, Ny and sample size. We used ImageJ software for the characterization of SEM image shown in Figure 2.7.

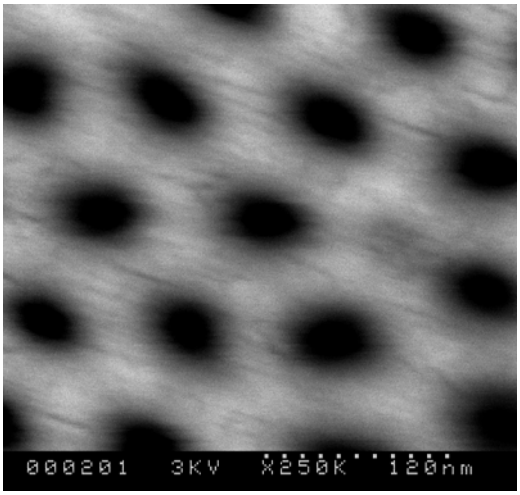

Figure 2.7 Image [66] used for calculating the pore density, pore inner and outer diameter using ImageJ software [45].

Table 2.1 Model parameters used in the simulation model.

Standard sample size	1 cm x 0.8 cm
Outer diameter do	40 nm
Number of CNTs in x-direction, N_x	1.27x10^5 pores
Number of CNTs in y direction, N_y	0.91x10^5 pores
Inner diameter of the pore, di	30 nm

The number of MWCNTs in x-direction, N_x and in y-direction, N_y and the inner and outer diameter were calculated for the image shown in Figure 2.7. We also measured the sizes of the sample and calculated the average value of all the parameters. The average values for all the parameters are mentioned in Table 2.1.

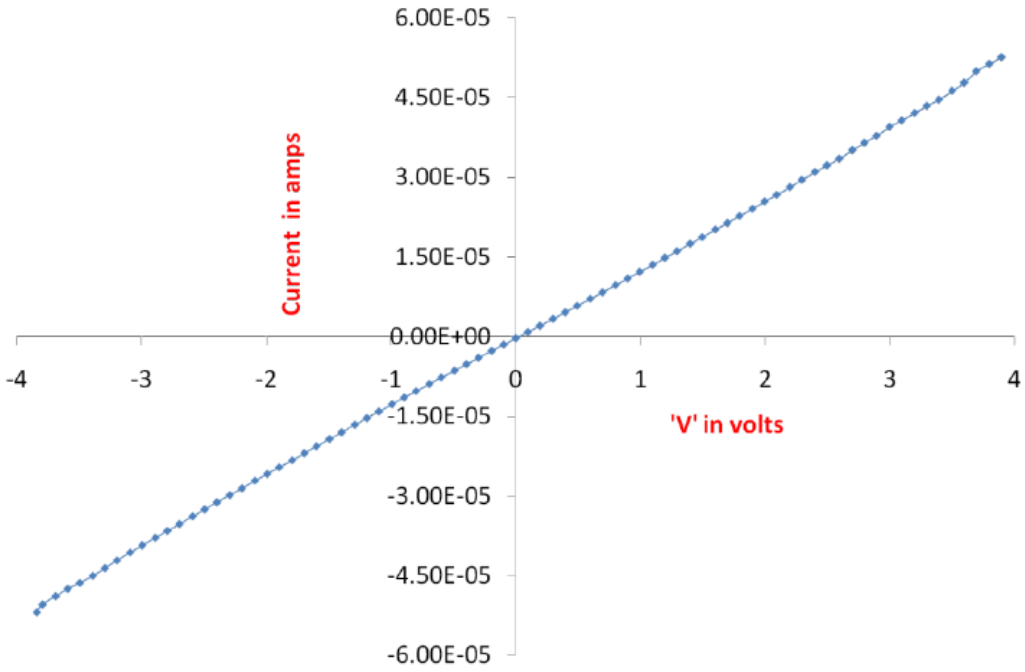

Figure 2.8:I-V measurements done at room temperature of the same batch of samples[73].

Table 2.2: Sample ρ_{CNT} calculation of batch sample rm_a_01.

Area of the sample	1x0.8 cm^2
Pore density=No. of pores/Area selected	106.5 pores / μm^2
Pore diameter	40nm,
Inner core diameter	30nm
Length of CNTs'	60 µm.
Area of the ring=π x [$(20nm)^2$- $(15nm)^2$] m^2	549.5 x10^-18 m^2

Neglecting contact resistance, taking parameter values from Table 2.2, we get

Average resistance of CNT from room temperature I-V characteristics of Figure 2.8

= dV/dI

(Slope of the I-V characteristics)= R_{CNT} =1.2 V/(1.5x10^-5 A) =85.7x10^3ohms

ρ_{CNT} = (R_{CNT} x Area of the ring)/(Length of the CNT)

= 85.7x10^3x π x [$(20)_2$- $(15)_2$]x10^-18 m^2 /60x10^-6 m= 7.8527E-005 ohm-cm

I-V measurements were done at room temperature to find the resistance of CNT by coating Pt on both sides of the sample.An ohmic behaviour was observed and the R_{CNT} calculation is shown below.This value of R_{CNT} of our device was used in the model discussed in section 2.8.

2.8 Model to analyze the steady state and transient response to ammonia molecules

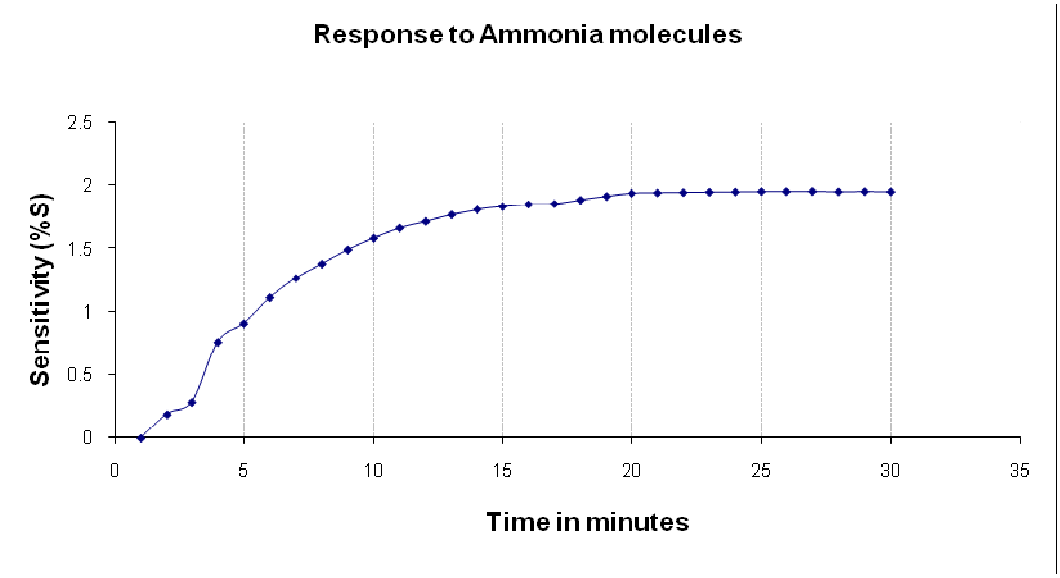

Figure 2.9: Sensor response to only 100 ppm ammonia at room temperature after initialization of 15 minutes of nitrogen carrier gas.

The test chamber was purged at a flow rate of 500 sccm at room temperature and relative humidity of about less 10 % with the test gas ammonia. Considering the flow of ammonia molecules into the test chamber started at time t=0, the sample would give transient response to the ammonia molecules and the sensitivity increased rapidly because of the resistance change of the sample upon the adsorption of ammonia molecules. Finally, after a few minutes as shown in Figure 2.9, the steady state is reached where all the adsorption sites of p-type semiconducting MWCNTs are assumed to be available to the electrons generated by the ammonia molecules which can be calculated by the true mass flow which helps in determining the resistance change and sensitivity due to the exposure of

ammonia molecules. Therefore,

Flow rate of Ammonia molecules in sccm into the test chamber = 500 sccm.

True Mass Flow =Flow rate in sccm x Gas density at standard room temperature

=500 cc/min x1L/1000cc x 0.76g/L

=0.38 g/min.

Number of moles of NH_3 gas= 0.38g/min/(17.03 g/mol)

= 0.0223 moles/min.

1 mole contains 6.023x10^23 molecules.

0.0223 moles contains 0.0223x6.023x10^23=0.134x10^23 molecules/min

No. of NH_3 molecules that comes into contact with CNT per min= N_1 .

1 NH_3 molecule will donate 0.04 electrons at the CNT surface to adsorb [60].

0.134x10^23 molecules/min will give 0.04x0.134x10^23 e^- per min.

No. of excess electrons generated, g =5.37x10^20 e^- per min.

T_1 is the electron lifetime for the recombination of holes of CNTs and electrons.

Number of electrons which get lost or do not recombine is Δn(t).

Therefore, the continuity equation is

$$\frac{-\Delta n(t)}{T1} + g = \frac{d\Delta n(t)}{dt} \qquad (2.10)$$

$$\Longrightarrow \frac{d\Delta n(t)}{dt} = \frac{g \times T1 - \Delta n(t)}{T1}.$$

Solving (2.10) we get

$$\Delta n(t) = g \times T_1 + c \times \exp\left(-\frac{t}{T_1}\right). \qquad (2.11)$$

At t=0 i.e. before the exposure of NH_3 molecules

Δn(t)=0.

Therefore,

$$c = -g \times T_1 = -5.37X10\text{^}20 \text{ per min} \times T_1 . \quad (2.12)$$

In steady state stage, the conditions are

$$\frac{d\Delta n(t)}{dt} = 0 \text{ and } \Delta n = n$$

and substituting these steady state conditions in (2.10), we get

$$n = g \times T_1 . \quad (2.13)$$

Before the exposure to ammonia molecules

$$\rho_{CNT} = (q \times \mu_p \times p_o)^{-1} \quad (2.14)$$

where p_o is the acceptor density concentration of p-type MWCNTs and μ_p is the mobility of the holes of MWCNTs in the template and using the value of ρ_{CNT} from page 16

$\mu_p = 10\text{^}4 \text{ cm}^2/\text{Vs}$ [63-65]

$\rho_{CNT} = (q \times \mu_p \times p_o)^{-1}$

$7.85x10\text{^}-5 \text{ ohm-cm} = 1/(1.6x10\text{^}-19x10\text{^}4x\ p_o)$

$p_o = 7.29x10\text{^}19 \text{ cm}\text{^}-3.$

After the exposure to ammonia molecules, the resistivity of CNT increases to

$$\rho'_{CNT} = (q \times \mu_p \times (p_o - n))^{-1} . \quad (2.15)$$

Substituting (2.15) in (2.9)

$$R'_{CNT} = \frac{4 \times \rho'_{CNT} \times h_{CNT}}{\Pi x(do^2 - di^2)} . \quad (2.16)$$

Using a rough approximation that

$R'_{dev}/R_{dev} = R'_{CNT}/R_{CNT}$

$= 0.89401/0.89162 = R'_{CNT}/85.7 \text{ x10\^4}$

$R'_{CNT} = 85.9 \text{ x10\^3 ohms.}$

Solving (2.13) ,(2.15) and (2.16) we get T1

$R'_{CNT} = 60 \text{ x10\^-6/((1.6 x 10\^-19x10\^4x(7.29x10\^19- 5.37x10\^20/60xT1)x549x10\^-18)}$

T1= 81.14 microseconds.

Substituting these values in (2.11) we get

c= -5.37x10^20 x 81.14x10^-6/(60 sec) =-7.2620 x10^14.

Therefore, $\Delta n(t)$= 7.262 x10^14x(1-exp(-t/81.14x10^-6) e^- per second . (2.17)

In this model, it was assumed that all the sites available for adsorption were being populated in the steady state concentration. However, there was a deviation in the theoretical and practical values because usually all the sites were not available for adsorption as there were some defects in formation of few CNTs. When the sample was plasma oxidized, the work function of MWCNTs changed [68] .The plasma also etched off the a-C layer from the tips of the nanotube in an anisotropic manner resulting in non uniform thickness of a-C layer. As a consequence, the calculation of the device resistance assuming that the a-C layer was covering whole of interpore region resulted in the deviation of measured device resistance from calculated device resistance.

The deviation in the experimental and theoretical values was due to the assumption that the a-C layer was continuous or of uniform thickness. Also, there were some defects in the CNTs formations which affected the number of sites available for the adsorption of ammonia molecules. Plasma etching of a-C layer by various techniques like water plasma, argon plasma and PECVD etch in oxygen also affected the tips of the CNTs in different ways and changed the work function in different manners [67-69]. Plasma etching of the top and bottom a- C layers results in the partial/complete removal of the a-C layer and change in the work function of MWCNT [67-69].

2.9 Comparison between experimental values of sensitivity measured and their theoretical values of device resistance

In this section, the experimental values of sensitivity and the theoretical values of device resistances are compared to calculate the least square error.

Table 2.3: Thicknesses of top and bottom layer of a-C before and after plasma etching.

Batch	As prepared		Plasma etched front 30s		Plasma etched back 30s	
	t_{top} in nm	t_{bot} in nm	t_{top} in nm	t_{bot} in nm	t_{top} in nm	t_{bot} in nm
Rm_a_01	28.3	30	0.164	30	0.164	0.030
Rm_a_210	12	12	0.475	11	0.475	0.063
Rm_a_02	8	12	0.481	20	0.481	0.028
Rm_a_03	16.4	16	0.167	35	0.167	0.026
Rm_a_04	35.6	35	0.768	13	0.768	0.024

Thin layer of a-C of thickness less than 10 nm cannot be measured reliably through the cross-sectional imaging feature of S-900.Therefore, the device resistance was calculated for various values of thicknesses of a-C layer in the simulation model and least square error (LSE) was calculated to get the best fit to the measured value of device resistance. Amorphous carbon layer thickness corresponding to the LSE fits are reported in Table 2.3. Next these values of thicknesses which gave the LSE, R_{CNT} and R'_{CNT} values obtained from (2.15) and (2.16) were used to calculate R_{dev} and R_{gas} before and after exposure to ammonia gas molecules using the simulation model discussed in Appendix A. Then sensitivity values were calculated using (3.4).

The SEM images of two devices rm_a_01 and rm_a_210 show that the thickness of a-

C layer is roughly about 30 nm and 20 nm for rm_a_01 and rm_a_210.

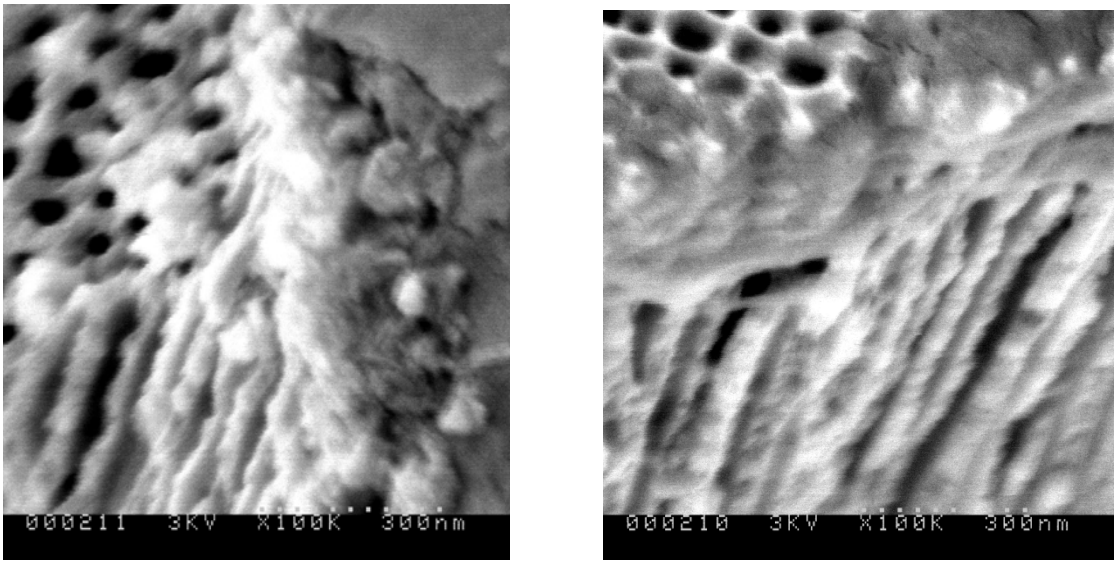

(a) (b)

Figure 2.10: Cross-sectional images of sample (a) rm_a_01 (b) rm_a_210.

Table 2.4(a) Comparison of theoretical and measured values of reference resistance of as prepared samples.

Batch sample	Calculated device resistance (R_{gas}) kΩ	Calculated device resistance (R_{dev}) kΩ	Measured resistance R_{ref} kΩ	LSE $(R_{dev}-R_{ref})^2$
rm_a_01	1.125	1.121	1.12	1x10^-6
rm_a210	2.827	2.822	2.82	4x10^-6
rm_a_03	1.937	1.932	1.93	2.5x10^-5
rm_a_04	0.893	0.891	0.89	1x10^-6
Rm_a_02	3.915	3.902	3.9	4x10^-6

Table 2.4(b) Comparison of theoretical and measured values of sensitivities of as prepared samples.

Batch sample	Sensitivity measured (%S)	Sensitivity calculated ($\%S_{cal}$)	LSE $=(\%S_{cal}-\%S)^2$
rm_a_01	0.4	0.36	1.6x10^-3
rm_a210	0.2	0.18	4x10^-4
rm_a_03	0.25	0.26	1x10^-4
rm_a_04	0.27	0.22	2.5x10^-3
Rm_a_02	0.33	0.32	1x10^-4

Table 2.5(a): Comparison of theoretical and measured values of reference resistance after the plasma etching of top side for 30 seconds.

Batch sample	Calculated device resistance (R_{gas}) kΩ	Calculated device resistance (R_{dev}) kΩ	Measured resistance R_{ref} kΩ	LSE $(R_{dev}-R_{ref})^2$
rm_a_01	79.889	75.011	75	1.21x10^-4
rm_a210	80.171	66.651	66.6	2.60x10^-3
rm_a_02	52.072	43.621	43.6	4.41x10^-4
rm_a_03	90.762	76.848	76.8	2.30x10^-3
rm_a_04	43.514	37.712	37.7	1.44x10^-3

Table 2.5 (b) Comparison of theoretical and measured values of sensitivity after the plasma etching of top side for 30 seconds.

Batch sample	Sensitivity measured (%S)	Sensitivity calculated ($\%S_{cal}$)	LSE $=(\%S_{cal}\%S)^2$
rm_a_01	6.5	6.56	3.6x10^-3
rm_a210	20.28	20.30	4.0x10^-4
rm_a_02	19.36	19.40	1.6x10^-3
rm_a_03	18.09	18.11	4.0x10^-4
rm_a_04	15.4	15.43	9.0x 10^-4

Table 2.6 (a): Comparison of theoretical and measured values of reference resistance after the plasma etching of top side and bottom for 30 seconds.

Batch sample	Calculated device resistance (R_{gas}) MΩ	Calculated device resistance (R_{dev}) MΩ	Measured reference resistance R_{ref} MΩ	LSE in R_{dev} $(R_{dev}- R_{ref})^2$
rm_a_01	1.1821	0.9817	0.98	2.89x10^-6
rm_a_210	0.6139	0.5017	0.5	3.24x10^-6
rm_a_02	1.4721	1.2013	1.2	1.69x10^-6
rm_a_03	1.4514	1.2157	1.2	2.46x10^-4
rm_a_04	1.5613	1.3071	1.3	5.04x10^-5

Table 2.6 (b) Comparison of theoretical and measured values of sensitivity after the plasma etching of top side and bottom for 30 seconds.

Batch sample	Sensitivity measured (%S)	Sensitivity calculated ($\%S_{cal}$)	LSE $=(\%S_{cal}-\%S)^2$
rm_a_01	19.47	19.43	1.6x10^-3
rm_a_210	21.40	21.48	6.4x10^-3
rm_a_02	22.51	22.56	2.5x10^-3
rm_a_03	20.09	20.01	6.4x10^-3
rm_a_04	18.19	18.22	9x10^-4

We observed in Table 2.4(b), Table 2.5(b) and Table 2.6 (b), the least square error was maximum of the order of 10^-3 in the measured and theoretical value of the calculated sensitivity because usually all the adsorption sites of the MWCNTs are not available for ammonia molecules. There was a deviation as detailed in Table 2.4 (a), Table 2.5(a) and Table 2.6 (a) in the calculated and measured reference resistance because there were some defects in the walls of the CNTs as seen in SEM images and also the presence of thin a-C layer is not continuous which blocks the pores of CNTs. Since, the a-C layers on top and bottom sides of the template were not uniform and continuous; the least square error would be there in the calculation of R_{top}, R_{bot} and device resistance R_{dev}.

Chapter 3 Experimental Procedures

3.1 Preparation of AAO template using anodization

The 2-step anodization process was performed in which the aluminum template was the anode, Pt electrode of a square shape of 1" was the cathode and the electrolyte used was 0.3 M Oxalic acid. The overall electrochemical cell set up for anodization is shown in Figure 3.1.

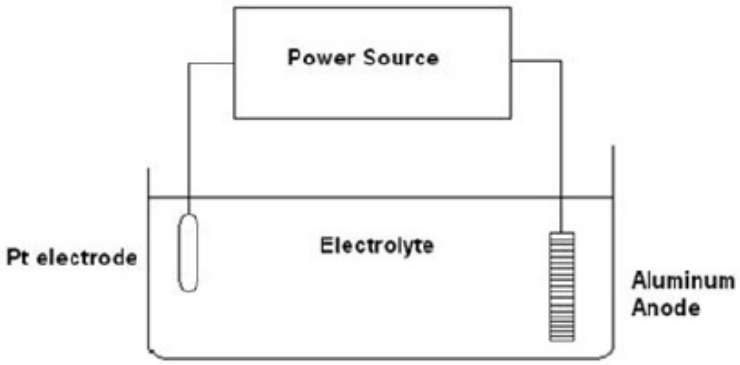

Figure 3.1: Electrochemical cell set up for anodization to prepare AAO template.

Chemical Reactions on Anode, Cathode and electrolyte solution are as follows:

At Anode: $2Al + 3\ H_2O \rightarrow Al_2O_3 + 6H^+ + 6e^-$. (3.1)

At Cathode: $6H^+ + 6e^- \rightarrow 3\ H_2$. (3.2)

Dissolution of Alumina: $Al_2O_3 + 6H^+ \rightarrow 2Al^{3+} + 3\ H_2O$. (3.3)

Chemical reactions for the processes at cathode and anode are explained in (3.1), (3.2) and (3.3).The Al tape was placed at the anode position in the electrochemical cell with Pt as the cathode [4].The electrolytes used for producing pores are generally weak or strong acids. A thick oxide or barrier layer (150-180 Angstroms) covered the metal surface

within seconds. This layer could be removed by partial dissolution in an acid at room temperature, leaving a well ordered pattern on grown Al_2O_3 pores. After this, a longer anodization step was performed to grow the pores in an ordered pattern over the remaining barrier oxide layer which served as an interface between the Al template and the electrolyte solution of 0.3M oxalic acid.

The highly pure (99.9 % pure Al) Aluminum tape was cleaned and degreased with organic solvents and was dried. Then, the cleaned and dry template was kept for 10 minutes in the electrochemical cell shown in Figure 3.1 with the voltage and the current supplied using a Kepco (Model ABC 125-1DM) programmable constant DC power supply at a low temperature. Since, the pores formed in this step were poor and not uniform, second anodization of longer duration of about 22 -24 hours was performed with same conditions used for the first anodization step. The samples were soaked now in acid solution for few hours until the remaining Al got etched off. The samples were now floated on acid for few minutes such that the barrier layer came in contact with the acid. The templates prepared by performing the above steps were annealed in oxygen in a lindberg furnace.

Pore size, pore density and depth of the anodized aluminum oxide layer can be controlled by changing experimental conditions in the electrochemical cell [27]. The choice of electrolyte could affect the pore diameter. Stronger acids tend to produce wider pores while weaker acids produce small pores [22, 25]. Current also affects pore dimensions when coupled with the electrolyte type or cell temperature [23].

3.2 MWCNTs growth by Chemical Vapor Deposition (CVD)

CVD is a common method for the commercial production of carbon nanotube. Chemical

vapor deposition is used for many applications such as fabricating semiconductor devices, deposition of layer coating etc. This process is commonly used for growing carbon nanotube with the presence of a metal catalyst. Nanotube grow at the sites of the metal catalyst; the carbon-containing gas is pyrolysed at the surface of the catalyst particle, and the carbon is transported to the edges of the particle, where it forms the nanotube. The catalyst particles can stay at the tips of the growing nanotube during the growth process, or remain at the nanotube base, depending on the adhesion between the catalyst particle and the substrate.

In our case, we did not use a catalyst to grow MWCNTs since the vertically grown pores of the Alumina template of 60 μm thick acted as a catalyst itself [28]. The porous alumina template fabricated above was used to grow vertically aligned MWCNTs in the pores. Pure xylene [$C_8H_{10}(C_6H_4C_2H_6)$] was used as the hydrocarbon source. A stream of nitrogen gas was purged at a controlled rate to minimize the turbulent flow of gas molecules in a Lindberg furnace of 96 mm diameter.

In this process, pyrolysis of xylene took place to produce carbon nanotube within the AAO pores without the use of catalyst for 1 hour. The furnace was then allowed to slowly cool in nitrogen [29].

A thin layer of amorphous carbon, a byproduct of CVD was also formed on both the sides of template whose thickness can be controlled by changing the CVD growth conditions by regulating the flow of nitrogen and temperature in the furnace. The layer of amorphous carbon formed mainly affects the sensor response and the resistance of the sensor and therefore, it was desirable to remove the amorphous carbon through plasma oxidation and Plasma Enhanced Chemical Vapor Deposition (PECVD).

3.3 Gas sensing system and sensitivity measurement

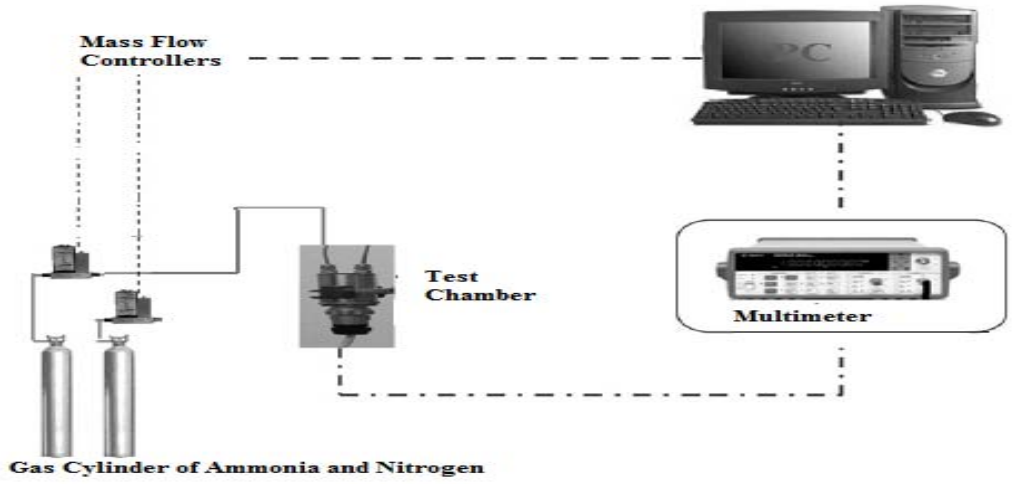

Figure 3.2: Gas sensing system [30].

MWCNTs were embedded in the pores of AAO templates and gold/silver bus bars were placed at both the edges of the sample to make electrical contacts so as to read the resistance change across the sample upon exposure to the test gas ammonia. For sensitivity measurement, we had the gas sensing system shown in Figure 3.2.The test gas 100 ppm ammonia and nitrogen gas cylinder were used with the precision Sierra instruments dual channel mass flow controller to control the flow rate into the glass sealed test chamber in which the sample was placed and the resistance change was measured using the HP 3478A digital multimeter. All the sensitivity measurements were done at room temperature at a flow rate of around 500 sccm and the relative humidity of the room was below 10%.The sensitivity, S(%) was calculated using :

$$S(\%) = \frac{(R_{gas} - R_{dev})}{R_{dev}} \times 100 \qquad (3.4)$$

where R_{dev} was the device resistance or reference resistance in the presence of carrier gas N_2 and R_{gas} was the resistance in the presence of the test gas ammonia.

Initially, the carrier gas nitrogen was purged into the test chamber having the sample for at least 15 minutes. Then, the test chamber was purged with alternate cycles of the test gas ammonia and nitrogen using the mass flow controller at flow rate of about 500 sccm at room temperature. After the first cycle of nitrogen and 100 ppm ammonia, UV light was emitted using the Black-Ray Long Wave Ultraviolet Light Model B 100AP (λ = 365 nm) along with the nitrogen cycle, so as to desorb the ammonia gas molecules. Kong *et al* proved that desorption of the analyte gas was required as the NH_3 gas molecules were chemisorbed on the MWCNT surface, thereby causing an upward drift in the reference resistance, as well as the sensitivity. Usually, desorption with heat and ultraviolet light are often employed to bring CNT sensors back to initial conditions [31].The sensor response for the cycling data and the steady state response is discussed in Chapter 4.

3.4 Plasma etching of a-C layer using microwave plasma oxidation

Microwave plasma oxidation was used for the plasma etching of the amorphous carbon layer. The sample was carefully placed in the plasma chamber and pumped down to a vacuum pressure of 30 milli Torr. The microwave was set to 75 W power. Oxygen gas [35-39] or argon gas [33][34] was then carefully injected into the chamber through a precision gas flow controller. Plasma oxidation was carried out in steps of 30 seconds on front and bottom sides of the sensor to reduce the thickness of a-C layer accordingly to analyze the current path through the conducting top and bottom layers of a-C and the MWCNTs. We observed through Scanning Electron Microscopy (SEM) of the sample that the a-C layer was etched off completely after the microwave plasma oxidation.

3.5 Plasma etching of a-C layer using Plasma Enhanced Chemical Vapor Deposition (PECVD) chamber.

In order to remove the amorphous carbon, plasma etching in oxygen plasma [35-39] and water plasma [40-42] were performed for 30 seconds on the front and back sides alternatively at a flow rate of 20 sccm and RF power of around 75 W in the PECVD chamber. The ammonia gas sensitivity was then measured after each step of 30 seconds of removal. The procedure of PECVD etch was to vent the vacuum chamber first fully to place the sample in it. The pump and the throttle valve were opened to allow the desired gas (oxygen and water vapor here) through the channel. The desired gas flow rate was set to 20 sccm. When the gas started flowing into the chamber, RF power was tuned for the desired oxygen or water plasma to form in the vacuum chamber having the sample. After desired amount of time, the RF power and gas flow were turned off .The chamber pressure was minimized by pumping it down. The sample was then removed from the vacuum chamber once the chamber was fully vented. We also observed that the a-C layer was etched off and higher sensitivities were recorded after PECVD etch.

3.6 Metal sputtering

The sputtering system can be used to deposit a variety of materials ranging from metals to metal alloys and oxides. The sample was placed in the vacuum chamber after venting it fully. The target (here 99.5% pure Nickel or Titanium) was placed on the gun. Inert gas like Ar was purged into the vacuum chamber at a flow rate of 15 sccm. The RF power was tuned to 75 W power. When the plasma was formed, a metal layer of 3 nm thickness was sputtered in the inert gas environment. After the deposition of the

metal layer of desired thickness on the sample, Ar gas flow was turned off and the vacuum chamber was pumped down. The sample was taken out from the chamber and the target was removed from the gun. After closing the chamber lid, the pump was turned on again.

In our study, metals of higher work function were chosen because they formed a good ohmic contact with the p type semiconductor MWCNTs of the template. Therefore, Ti and Ni metals were used to sputter top and bottom sides of the template after the removal of a-C layer through the above mentioned plasma etching techniques to study the current flow.

3.7 Scanning Electron Microscopy (SEM)

The scanning electron microscope (SEM) is an electron microscope which images the sample surface by raster scanning with a high-energy beam of electrons. The electrons interact with the atoms of the sample producing signals that contain information about the sample's surface morphology, composition, and other properties. It can produce very high resolution images of small size samples of up to 5 nm and can have a wide range of magnifications.

A Hitachi Field Emission Scanning Electron Microscope (Model S-900) with a maximum magnification power of 800kX was used for characterizing MWCNTs embedded in AAO templates for cross-section of the images and also for studying the top and bottom morphology of AAO templates. To characterize the image of a particular sample, a very small section of the sample was cut-off from the original sample and mounted on a double-sided sticky carbon tape stuck on a SEM stub. The sample was coated with colloidal graphite on the edges and Gold-Palladium alloy was sputtered to

ensure proper electrical conductivity throughout the sample. Specimens were imaged for both topology and cross-sectional views which helped in calculating the pore diameters and inter-pore distances. The amorphous carbon layer thickness was also measured by tilting the sample to an angle of 20 º to 30 º using the cross-sectional imaging feature of S-900.

Chapter 4 Results and Discussions

4.1 Improvements in the design for sensitivity enhancement

As discussed earlier in Chapter 2, the device can be considered as having two current paths the direct current path between the bus bars through the top conducting layer of a-C and the alternate path through the CNTs and bottom conducting layer of a-C. The current should flow through the latter path to obtain a higher sensitivity since the CNTs were mostly involved in the sensing mechanism.

Therefore, the device configuration to get the highest sensitivity to ammonia molecules should be as follows:

- Conceptually, the device becomes sensitive to gas species when the direct current path becomes too resistive and the current chooses the alternate path.
- The device configuration should be such that the alternate path is preferred, but current should be spread out so that the nanotubes are involved in sensing mechanism.
- If the MWCNTs are not carrying current, they do not contribute to the device resistance change & therefore do not affect the sensitivity.
- As prepared samples with bus bar contacts deposited on the thinner layer of a-C, such that $R_{Top} > R_{Bot}$, will yield a higher sensitivity than samples with the bus bars on the thick a-C layer($R_{Top} < R_{Bot}$).
- A modified bottom layer to reduce the resistance of R_{Bot} will yield higher sensitivity**.**

- The amorphous carbon on the bottom and top layers of the sample act as electrical contact between the tubes and the top layer is less resistive for as grown samples due to which it will yield poor sensitivity**.**

Varying the thickness of the a-C layer on top and bottom by the following methods would yield higher sensitivities:

- Making the thickness of the top and bottom a-C layer of comparable thickness.
- Decreasing the thickness of the top layer to less than the thickness of the bottom layer i.e. $R_{top} > R_{Bot}$.
- Removing the a-C layer on the top and bottom sides of the template and replacing it with a higher conductive layer by metal.

The sensing results obtained after tailoring with the thickness of the a-C carbon layer on top side and bottom side with various techniques of plasma etching of a-C are discussed in section 4.2.

4.2 Sensitivity observed after microwave plasma oxidation

The sensor response is given by the formula:

$$S(\%) = \frac{(R_{gas} - R_{dev})}{R_{dev}} \times 100$$

where R_{dev} is the device resistance or reference resistance in the presence of carrier gas N_2 and R_{gas} is the resistance in the presence of the test gas ammonia.

4.2.1. Sensitivity observed for microwave plasma oxidation in oxygen

The sensor developed in AAO templates were highly responsive to ammonia molecules and the lower response time and recovery times were observed as shown in

Figure 4.1

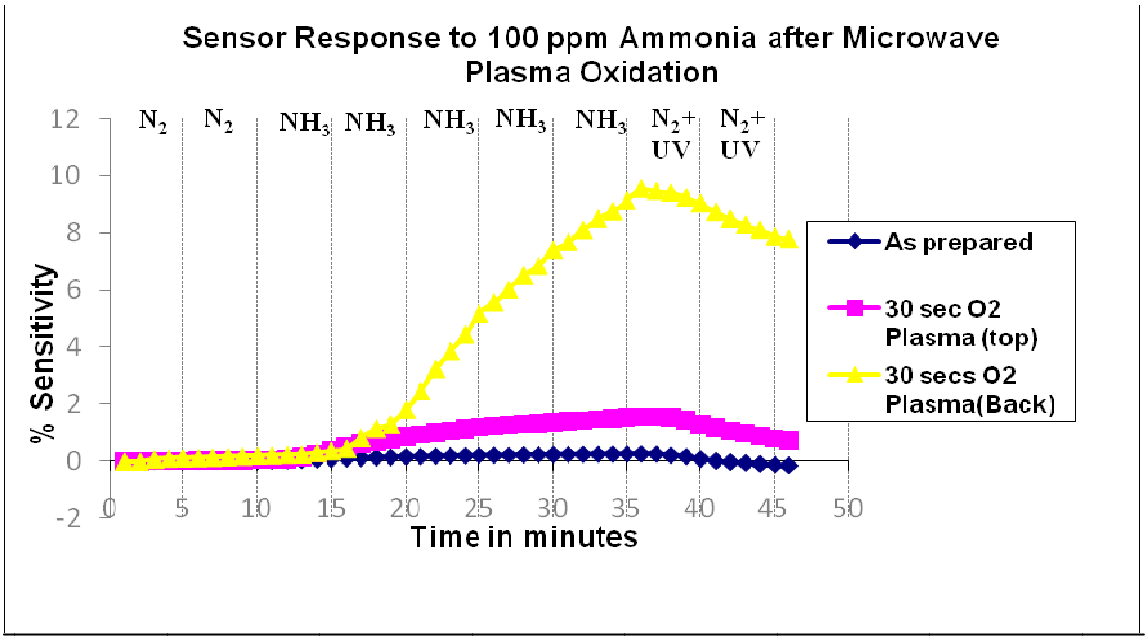

Figure 4.1: Sensor response to 100 ppm ammonia after microwave plasma oxidation in oxygen.

For the first ten minutes, the sample was exposed to nitrogen gas as the carrier gas and then we injected the test gas, 100 ppm ammonia (NH_3) gas for the next 25 minutes until 35 minutes where peak sensitivity was observed as the sample reaches the steady state or saturation level. After 35 minutes, we injected the nitrogen gas for the next 10 minutes in the presence of Ultra Violet (UV) light using the Black-Ray Long Wave Ultra Violet Light Model B 100AP (λ = 365 nm) for desorption. Desorption of the analyte gas was required because the NH_3 gas molecules were chemisorbed on the MWCNT surface, which caused an upward drift in the reference resistance as well as the sensitivity. Therefore, a high binding energy like UV light was required to desorb the analyte gas molecules to bring back the MWCNTs to its initial conducting state [53].

Table 4.1: Results of microwave plasma oxidation in oxygen.

As prepared sample	
Reference resistance	2.82 kohms
Sensitivity	0.26%.
Microwave plasma oxidation in oxygen performed for 30 seconds on the front side	
Reference resistance	16.8 kohms
Sensitivity	1.56 %
Microwave plasma oxidation in oxygen performed for 30 seconds on the back side	
Reference resistance	1.07 Mohms
Sensitivity	9.53%

Discussion:

The highest sensitivity according to Table 4.1 after the microwave plasma oxidation in oxygen done in steps of 30 seconds for the front and back side of the sample was 9.53% which proved that after the removal of a-C layers [56-59] on top and bottom sides would yield a higher sensitivity.

4.2.2 Microwave plasma oxidation in argon:

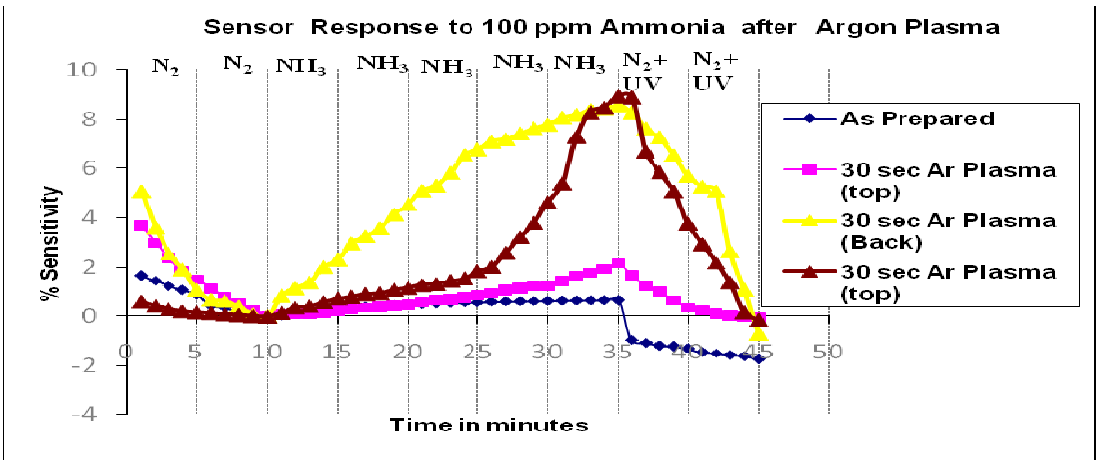

Figure 4.2: Sensor response to 100ppm ammonia after microwave plasma oxidation in argon.

Table 4.2: Results of microwave plasma oxidation in argon gas.

As prepared sample	
Reference resistance	185 ohms
Sensitivity	0.65%.
Microwave plasma oxidation in argon performed for 30 seconds on the front side	
Reference resistance	6.6 kohms
Sensitivity	2.13 %
Microwave plasma oxidation in argon performed for 30 seconds on the back side	
Reference resistance	94 kohms
Sensitivity	8.57%
Microwave plasma oxidation in argon performed for 30 seconds on the front side	
Reference resistance	0.54 Mohms
Sensitivity	8.95 %

Discussion:

Since, it had been found that argon gas ions knocked out the a-C layer on top and bottom sides of the sample [54, 55], thus helping in the removal of the amorphous carbon from the samples and enhancing the sensitivity as seen in Figure 4.2.

As compared to microwave plasma oxidation in oxygen, we can say that plasma oxidation in argon was not as effective as that in oxygen in removing the layer of a-C carbon according to the sensitivity results in Table 4.1 and Table 4.2.

4.3 Sensor response after Plasma Enhanced Chemical Vapor Deposition (PECVD) etch in oxygen

Another technique to remove a-C layer on the top and bottom layers of the sample to yield good sensitivity is Plasma Enhanced Chemical Vapor Deposition (PECVD) etch in oxygen and was used for the first time to remove a-C layer for enhancing the sensitivity of CNT based resistive sensor.

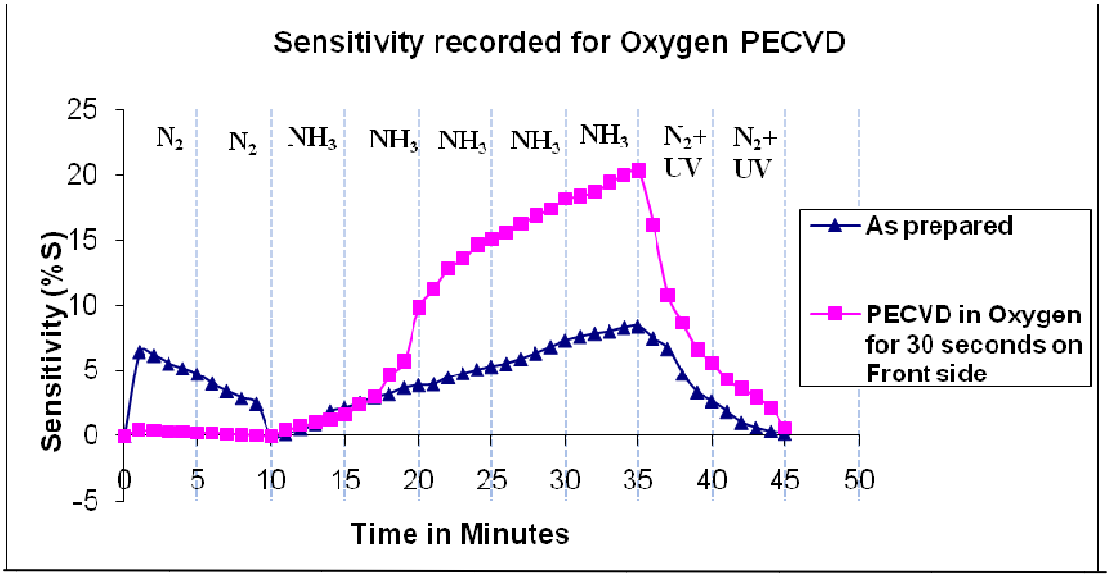

Figure 4.3: Sensor response to 100 ppm ammonia after PECVD etch in oxygen.

Table 4.3: Results of PECVD etch in oxygen.

As prepared sample	
Reference resistance	0.56 kohms
Sensitivity recorded	8.3%
PECVD etch in oxygen under pristine conditions for 30 seconds on the front side	
Reference resistance observed	66.6 kohms
Sensitivity measured	20.3 %

Discussion:

In order to remove the amorphous carbon, PECVD etch in oxygen plasma [35-39] was performed for 30 seconds on the front and back sides alternatively at flow rate of 20 sccm and RF power of around 75 W and then measured the ammonia gas sensitivity after each step of 30 seconds of removal. The capacitively coupled plasma formed in the PECVD chamber at pressure of few Torrs yielded a better result in the removal of a-C layer which can be shown in the images in Figure 4.4.

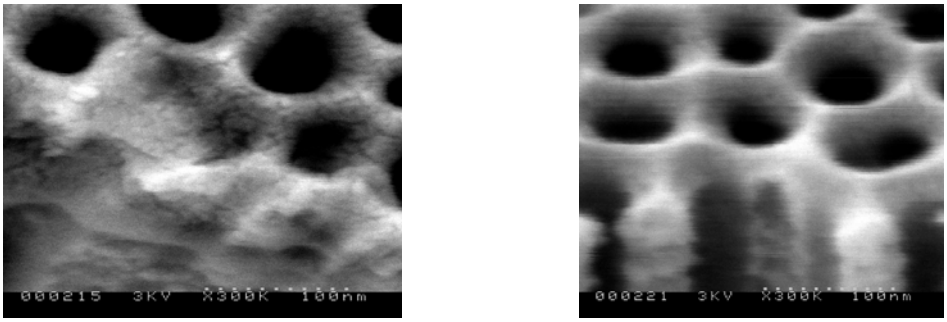

(a) (b)

Figure 4.4: Images of sample (a) after 30 seconds of PECVD etch in oxygen (b) after 1 minute of PECVD etch.

It can be seen in the images that after PECVD etch in oxygen, the layer of a-C was almost fully removed and sensitivity results improved according to Table 4.3.

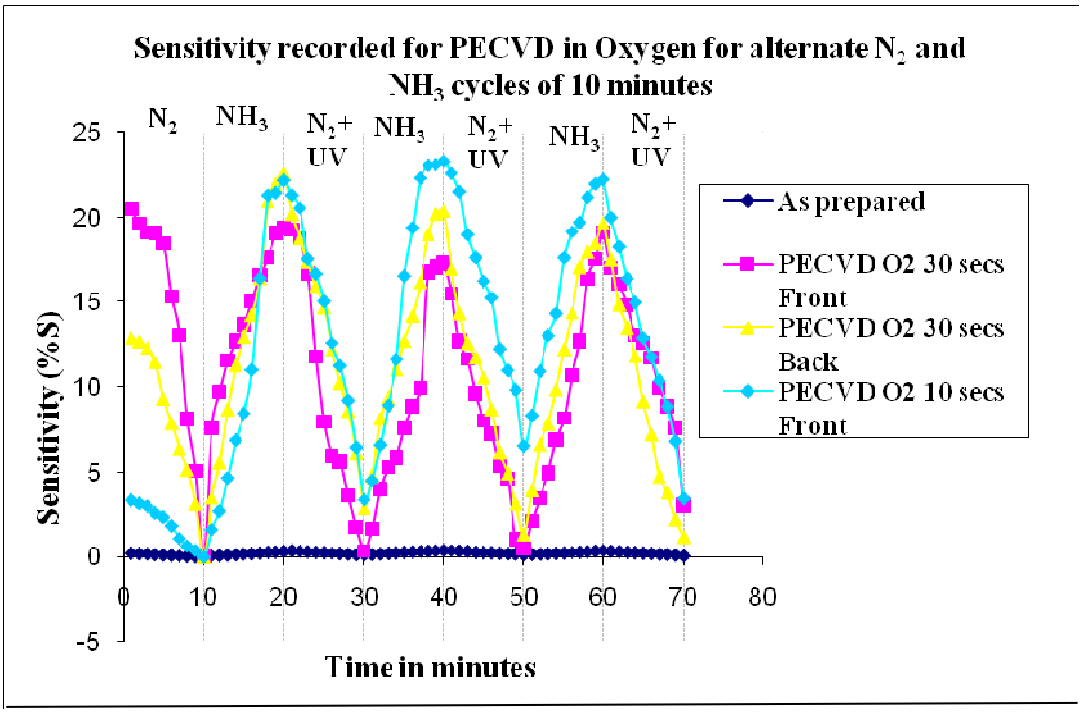

Figure 4.5: Sensor response to 100 ppm ammonia at room temperature to cycles of nitrogen and ammonia.

Table 4.4: Results of PECVD etch in oxygen for alternate cycles of nitrogen and ammonia.

As prepared	
Reference resistance	3.92 kohms
Sensitivity	0.39%
PECVD etch in oxygen 30 s on the front side	
Reference resistance	43.66 kohms
Sensitivity	19.36 %
PECVD etch in oxygen 30 s on the back side	
Reference resistance	1.24 Mohms
Sensitivity	20.34 %
PECVD etch in oxygen for 10 s on the front side	
Reference resistance	1.55 Mohms
Sensitivity	23.2 %

Discussion:

The sensor response to 100 ppm ammonia is shown in Figure 4.5 and detailed in Table 4.4 for the alternate cycles of carrier gas nitrogen and test gas ammonia which gave sensitivity as good as that of SWCNT sensor claimed so far for SWNT-PABs composite sensor to 0.01% ammonia of 22% [59].

4.4 Water plasma etch

Another way to etch off the a-C layer was water plasma etch [41],[42].We were the first group to use water plasma to etch off the a-C layer and use this technique for enhancing the sensor response to 100 ppm ammonia. Water plasma etch was performed on the front and back side for 30 seconds to remove the a-C layer on top and bottom sides at a flow rate of 20 sccm and pressure of few Torr. The RF power was tuned to about 75W.

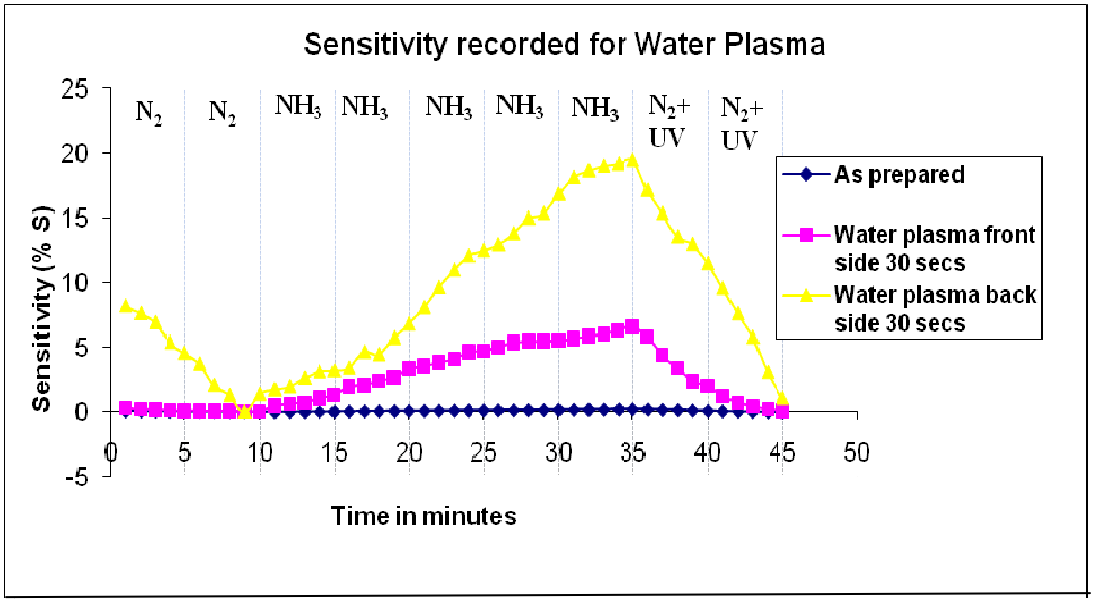

Figure 4.6: Sensor response to 100 ppm ammonia after water plasma etch.

Table 4.5: Results of water plasma etch.

As prepared	
Reference resistance	1.1 kohms
Sensitivity	0.22 %
Water Plasma etch for 30 seconds on the front side	
Reference resistance	75.4 kohms
Sensitivity	6.57%
Water Plasma etch for 30 seconds on the back side	
Reference Resistance	0.98 Mohms
Sensitivity	19.5%

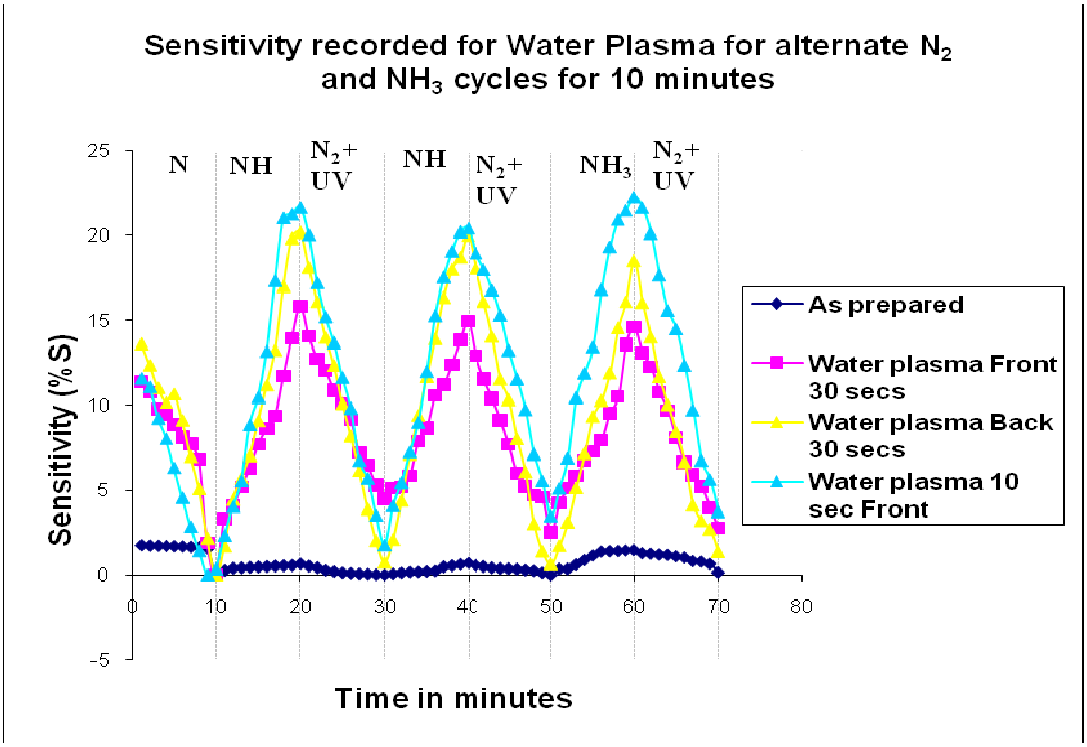

Figure 4.7 (a): Sensor response to 100 ppm ammonia at room temperature for alternate cycles of nitrogen and ammonia after water plasma etch.

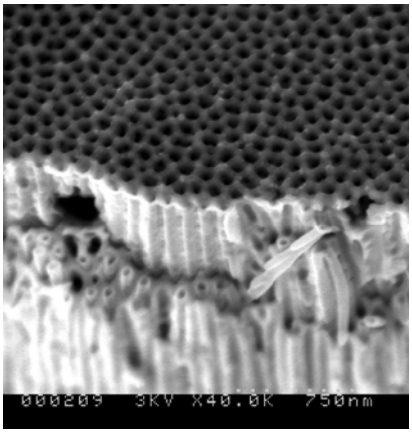

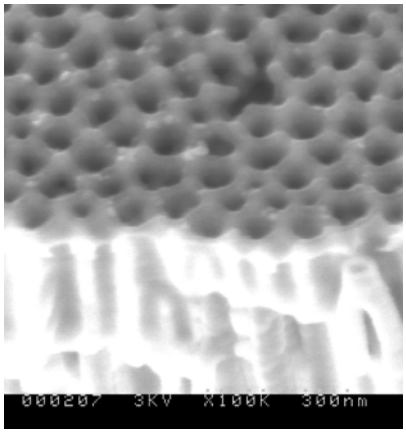

Figure 4.7 (b): Images after water plasma of the front side of the sample.

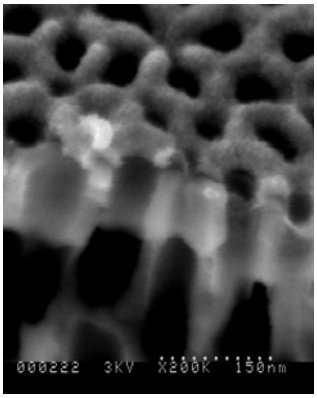

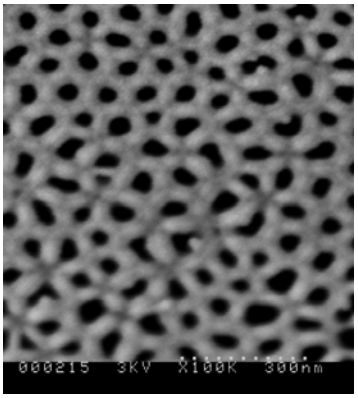

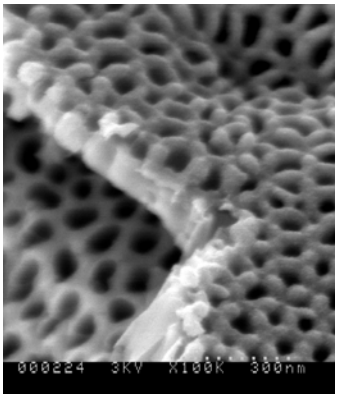

Figure 4.7 (c): Images after water plasma of the back side of the sample.

Discussion:

Sensitivity for the as prepared sample having a reference resistance of 4.38 kohms was 1.5%. After performing water plasma etch for 30 seconds on the front side of the sample, the sensitivity and reference resistance shoot up to 15.8% and 21.96 kohms. After performing the water plasma etch for 30 seconds on the back side of the sample, the reference resistance and sensitivity increased to 0.98 Mohms and 19.5 % respectively as detailed in Table 4.5. To enhance the sensitivity water plasma etch was again performed for 10 seconds only on the front side and we observed a higher sensitivity of 22.2 % as good as that of SWNT sensors according to Table 4.6. It can also be seen in images

above that a-C layer has been removed after the water plasma etch.

Table 4.6: Results of water plasma etch for alternate cycles of ammonia and nitrogen.

As prepared	
Reference resistance	4.38 kohms
Sensitivity	1.5%
Water plasma etch for 30 seconds on the front side	
Reference resistance	21.9 kohms
Sensitivity	15.8 %
Water plasma etch for 30 seconds on the back side	
Reference resistance	1 Mohms
Sensitivity	20.3%
Water plasma etch for 10 s on front side	
Reference resistance	1.2 Mohms
Sensitivity	22.2%

Comparison of various plasma etching techniques:

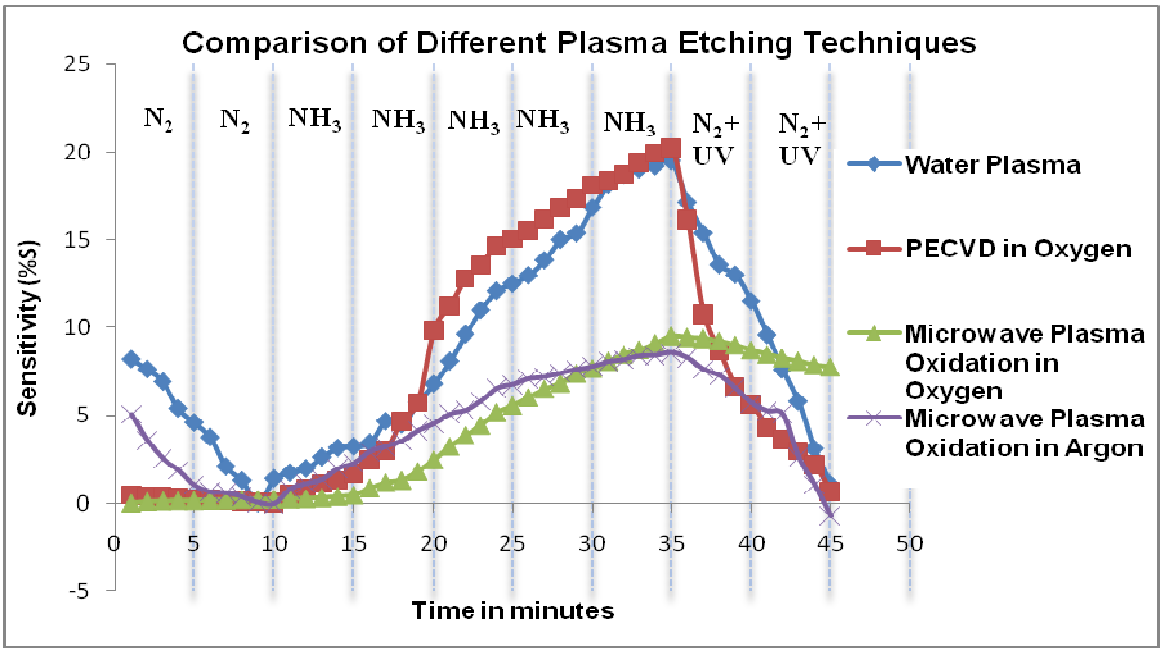

Figure 4.8: Comparison of various plasma etchniques after etching the a-C layer for 1 minute on one side.

The sensitivity recorded at room temperature to 100 ppm ammonia after performing PECVD etch in oxygen for one minute was 20-22% whereas for water plasma etch was 15- 20 %.The sensitivity recorded after microwave plasma oxidation in oxygen and argon were 9 and 8 % respectively.The sensitivities recorded after PECVD etch and water plasma etch were higher as compared to that measured after microwave plasma oxidation because the PECVD and water plasma were done at a lower pressure, high vacuum and pristine conditions according to Figure 4.8.However, the binding energy and work function of the nanotube decreases [67-69] which is responsible for improving the sensitivity.

4.5 Sputtering with a metal

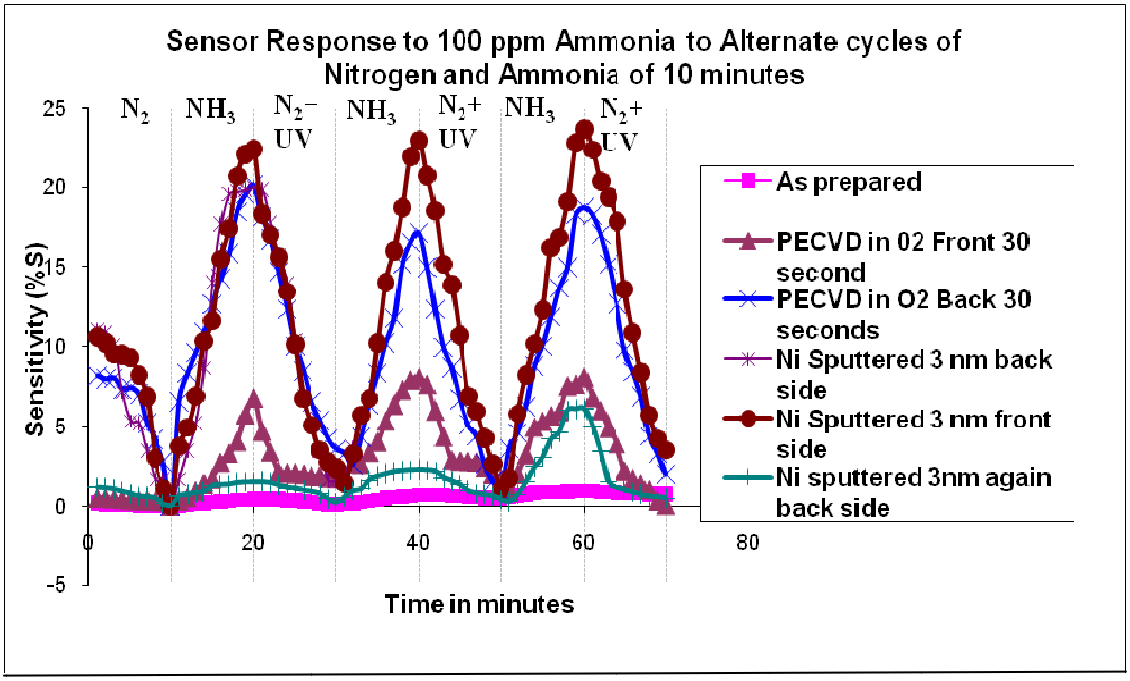

Figure 4.9: Sensor response to 100 ppm ammonia at room temperature after the metal sputtering.

Table 4.7: Results of Ni sputtered sample exposed to 100 ppm ammonia.

As prepared sample	
Reference resistance	2.17 kohms
Sensitivity	0.92 %
PECVD etch in O_2 done on the front side for 30 seconds	
Reference resistance	76.8 kohms
Sensitivity	8.11%
PECVD etch in O_2 done on back side for 30 seconds	
Reference resistance	1.20 Mohms
Sensitivity	20 %
Ni sputtered on the back side 3 nm	
Reference resistance	0.58 Mohms
Sensitivity	19.98%
Ni sputtered on front side 3 nm	
Reference resistance	59.35 kohms
Sensitivity	17.93%
Ni sputtered again 3nm front (total 6 nm)	
Reference resistance	3.5 kohms
Sensitivity	6.19%

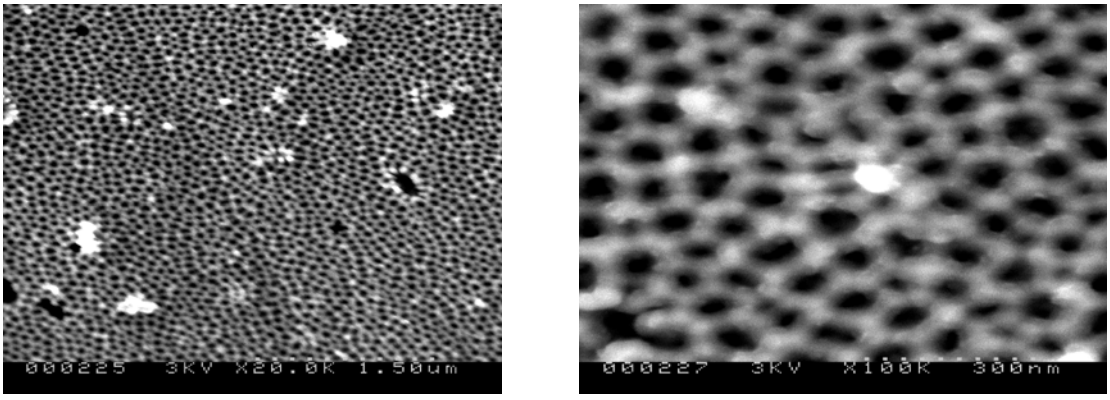

Figure 4.10 Images after Ni sputtering of the front side of the sample.

Discussion:

The sensor gave a better response of about 19.98 % according to Table 4.7 to ammonia with the decreasing thickness of a-C layer and after removing the a-C layer and sputtering the back side with metal of higher work function than that of CNTs. This sputtered metal behaved as a conducting layer between the CNTs of the model through which the current can pass through the alternate path through the CNTs. When the metal was sputtered on the front side of the sample, then the sensitivity decreased to 17.3 % because the current directly flowed through the direct path between the bus bars of the CNTs without involving the CNTs according Table 4.7. The sensitivity would also decrease with the increasing thickness of the metal layer as the pores of the template will be blocked by the metal layer, thereby decreasing the availability of CNT sites for adsorption of the ammonia molecules.

When we removed the a-C layer and then replaced it with the resistivity of the metal in our simulation model developed to calculate the device resistance as discussed in program given in Appendix would also give the appropriate result with the practical values obtained for the device resistance with a deviation. The least square error was mainly because the sputtered film of metal was not continuous and of the exact thickness 3 nm as we sputtered as seen in Table 4.10.

According to the basic theory of metal/semiconductor interface, the p-type semiconducting CNT can form an ohmic contact with a metallic electrode when $\varphi M > \varphi S$, where φM and φS are the work functions of the metallic electrode and the semiconducting CNT, respectively. On the other hand, a metallic electrode having a lower work function than φS may form a schottky barrier at the metal/CNT contact. In

contrast to this, the n-type semiconducting CNT could form the schottky barrier when $\varphi M > \varphi S$ [67].The work function of Ti and Ni are 4.33 eV and 5.05 eV respectively which forms an ohmic contact with the CNTs. The work function of CNT according to literature is approximately equal to 4.4 eV which decreases after the plasma etching steps to 4.2 eV [68-71]. The sensor response after the metal sputtering also shows that the CNTs show p-type behavior.

Ti sputtering results:

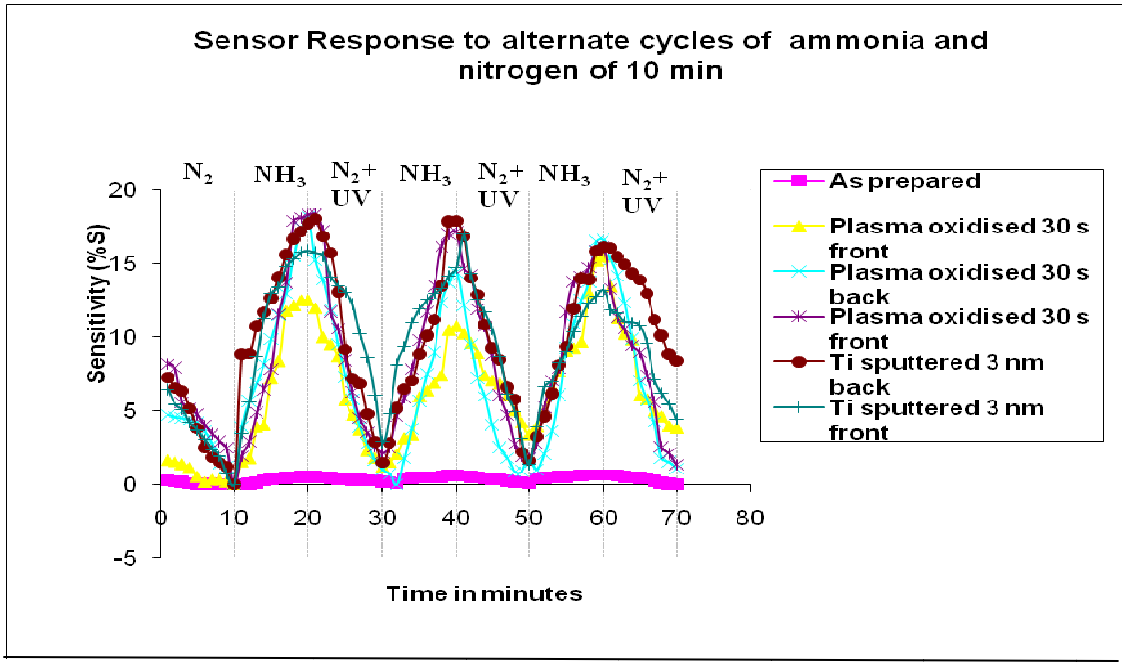

Figure 4.11: Sensor response to 100 ppm ammonia at room temperature.

Table 4.8: Results of Ti sputtered sample when exposed to 100 ppm ammonia.

As prepared	
Reference resistance	1.18 kohms
Sensitivity	0.64%
Plasma oxidized for 30 seconds on the front side	
Reference resistance	37.6 kohms
Sensitivity (%S)	10.73%
Plasma oxidized for 30 seconds on the back side	
Reference resistance	1.23 Mohms
Sensitivity	18.19%
Ti sputtered 3nm on the back side	
Reference resistance	0.56 Mohms
Sensitivity	18.37 %
Ti sputtered 3 nm on the front side	
Reference resistance	43.16 kohms
Sensitivity	17.74 %
Ti sputtered 3 nm on the back side	
Reference resistance	1.44kohms
Sensitivity	15.89 %

Discussion:

After removing the a-C layer, it can be seen that the resistance decreases with the Ti metal deposition whose electrical resistivity is 0.42 μohm-m [71] and when we deposit the metal on the back layer the sensitivity increases a little because it facilitates the current flow in the device. When the metal layer is deposited on the top side, then there would be a great decrease in the sensitivity as the current would follow the direct path of low resistive metal Ti layer as seen in Table 4.8. Therefore, the device configuration

should be such that the current follows the alternate path involving the MWCNTs.

Comparison of Ni and Ti sputtering results:

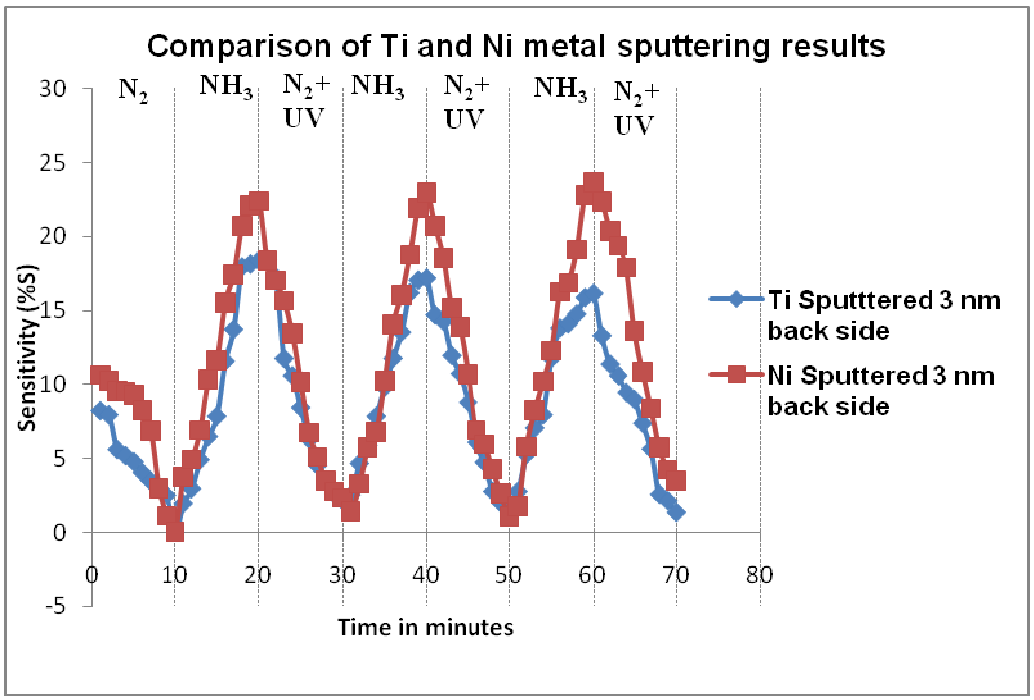

Figure 4.12: Comparison of Ni and Ti sputtering results after the deposition of 3 nm on the back side.

4.6 Results of the simulation model after calculating the R_{top} and R_{bot} due to metal layer Ni and Ti Metal:

Table 4.9: Model parameters used in simulation model.

Resistivity of Ni	69.3 µohm-cm [71]
Resistivity of Ti	0.42 µohm-m [72]
Standard sample size	1 cm x 0.8 cm
Outer diameter do	40 nm
Inner diameter of the pore di	30 nm
Resistivity of amorphous carbon	1.55x10^-3 ohm-cm [46-49]
Resistance of the MWCNTs	85.7 kohms
Number of CNTs in x-direction	1.27x10^5
Number of CNTs in y direction	0.91x10^5

The parameters in Table 4.9 were used to calculate the device resistance using the simulation model for a range of thicknesses of top and bottom layer of a-C/ metal layer according to the sensing experiments done. Least square error was calculated to get the best fit to the measured values of device resistance as shown in Table 4.10. The Ni and Ti sputtering were done on the device rm_a_03 and rm_a_04 respectively after removing the a-C layer by plasma etch process. Therefore the thickness of a-C layer was taken from Table 2.3 for device rm_a_03 and rm_a_04.The remaining layer of a-C was fully removed by plasma etch process and then sputtered with the metal layer.

Table 4.10: Simulation results for calculating R_{dev} with metal layer on top and bottom.

Thickness of top layer (t_{top})	Thickness of bottom layer (t_{bot})	Calculated R_{dev}	Measured device resistance R_{ref}	LSE (R_{dev}-R_{ref})^2
0.167 nm a-C	0.08 nm Ni	0.55 Mohms	0.58 Mohms	1.6x10^-3
0.08 nm Ni	0.08 nm Ni	59.18 kohms	59.35 kohms	2.89x10^-2
0.16 nm Ni	0.08 nm Ni	3.64 kohms	3.50 kohms	1.96x10^-2
0.77 nm a-C	0.07 nm Ti	0.54 Mohms	0.56 Mohms	4x10^-4
0.07 nm Ti	0.07 nm Ti	44.71 kohms	43.16 kohms	3.03x10^-3
0.07 nm Ti	0.21 nm Ti	1.49 kohms	1.44 kohms	2.5x10^-3

4.7 Results of the simulation model and comparison with the experimental values:

The model parameters for a batch of sample for the image shown in Figure 2.8 are in Table 4.11.Taking resistivity of amorphous carbon as 1.55x10^-3 ohm-cm [46-49] and the resistance of the MWCNTs calculated was 85.7 kohms.

Table 4.11: Showing the simulation results of MATLAB program to calculate the device resistance of the resistive sensor model using the R_{CNT} value as 85.7 kohms.

Thickness of top a-C ($t_{ac,top}$)	Thickness of bottom a-C ($t_{ac,bot}$)	R_{top} (ohms)	R_{bot} (ohms)	R_{dev} (ohms) calculated
30 nm	30 nm	668.6171	668.6171	1090
20 nm	20 nm	1.003+E03	1.003+E03	1664
10 nm	10 nm	2.01E+03	2.01E+03	3512
1 nm	1 nm	2.01E+04	2.01E+04	31607
0.5 nm	0.5 nm	4.01E+04	4.01E+04	63210
0.01 nm	0.01 nm	2.01E+06	2.01E+06	316070

Table 4.11 was generated for a range of values of thickness to get a rough estimate of the device resistance with respect to top and bottom thicknesses of a-C layer using the simulation model discussed in Appendix.

The results in the Table 4.11 were in accordance with the experimental values of device resistance. The device or reference resistance for the as prepared sample having the a-C layer of thickness around 10- 30 nm would usually have the resistance around 500 ohms to 2 kohms which proved that the resistance of the top and bottom layers R_{top} and R_{bot} is inversely proportional to the thickness of the amorphous carbon according to (2.9).

4.8 Variation of resistance of top and bottom a-C layers with the thickness of a-C layer

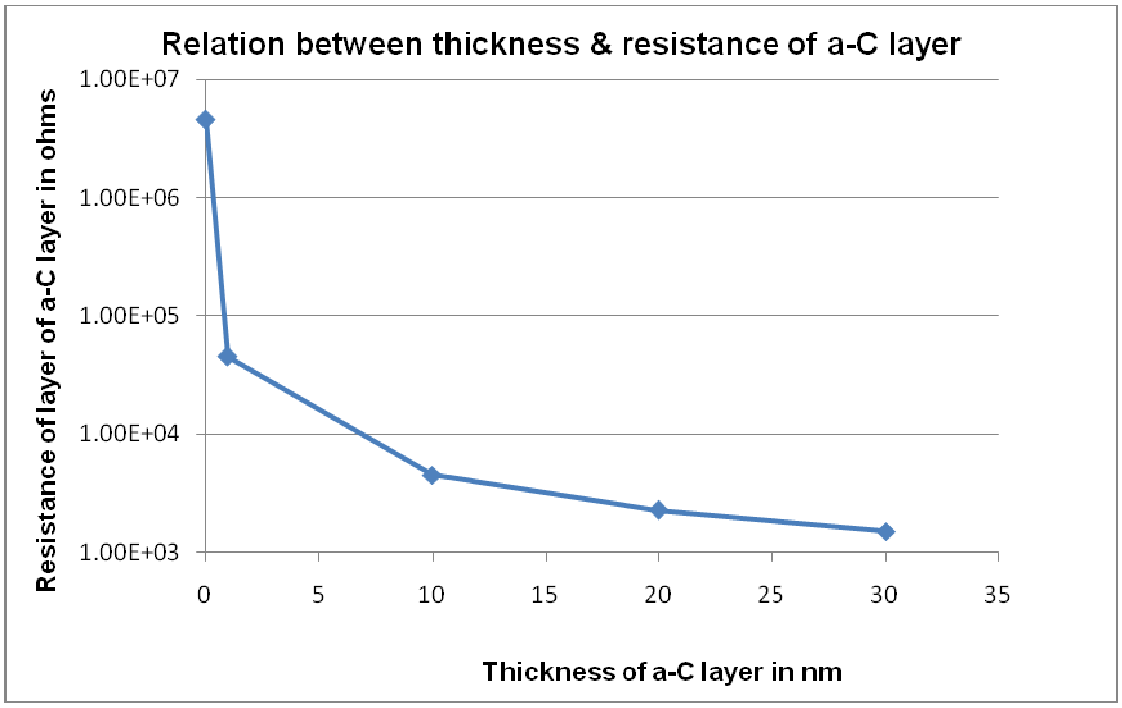

Figure 4.13: Relation between a-C layer thickness and resistance R_{top} or R_{bot} with resistivity of a-C layer as 3.5x10^-3 ohm-cm.

Another set of results for a different value of the resistivity of amorphous carbon stated in [48] is shown in Table 4.12.Taking resistivity of amorphous carbon as 3.5 x10^-3 ohm-cm [46-49] and the resistance of the MWCNTs as calculated as 85.7 kohms.

Table 4.12: The simulation results for different value of resistivity of amorphous carbon of 3.5x10^-3 ohm-cm.

Thickness of top a-C ($t_{ac,top}$)	Thickness of bottom a-C ($t_{ac,\ bot}$)	R_{top} (ohms)	R_{bot} (ohms)	R_{dev} (ohms)
30 nm	30 nm	1.51E+03	1.51E+03	1.05E+03
20 nm	20 nm	2.26E+03	2.26E+03	1.58E+03
10 nm	10 nm	4.53E+03	4.53E+03	3.16E+03
1 nm	1 nm	4.53E+04	4.53E+04	3.16E+04
0.5 nm	0.5 nm	4.01E+04	4.01E+04	2.8E+04
0.01 nm	0.01 nm	4.53E+06	4.53E+06	3.16E+06

4.9 Variation of device resistance with the resistance of layer of amorphous carbon R_{top}/R_{bot}

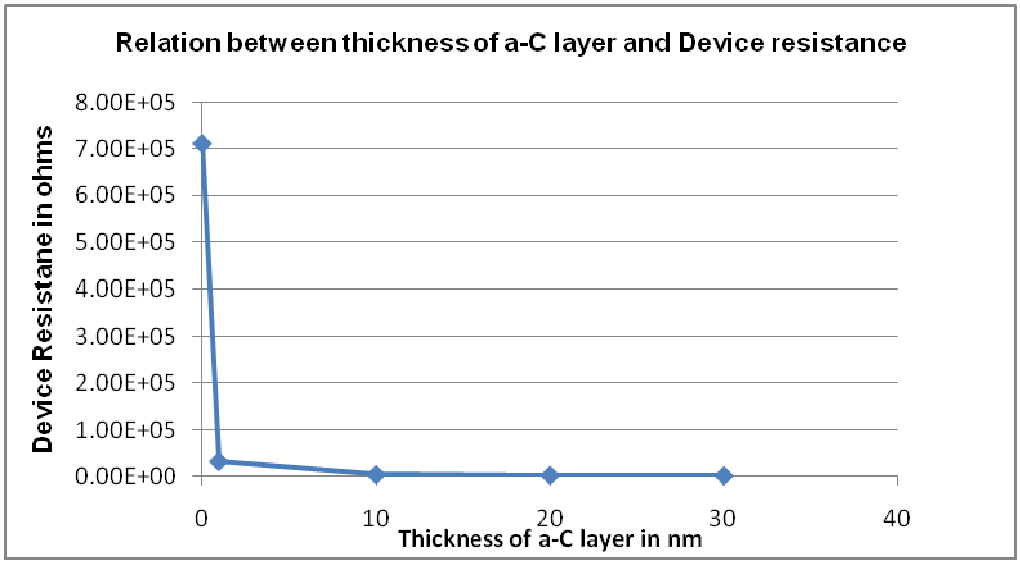

Figure 4.14: The variation of device resistance with the thickness of a-C layer on top/bottom side for the values in Table 4.12.

We can see in Figure 4.14 that the thickness of the a-C layer is inversely proportional to the resistance of the top/bottom layer of a-C.

Estimated values of thickness of a-C layer after PECVD etch in oxygen for the batch of sample of rm_a_03 are in Table 4.13.

Table 4.13: Estimated values of thickness of a-C layer after plasma etching off the a-C layer by PECVD in oxygen layer and the according to simulation results.

Condition	Thickness of a-C layer (nm)	Reference resistance	% Sensitivity
As prepared	20	2.17 kΩ	0.97
30 s PECVD etch in O_2	10	76.8 kΩ	8.11
60 s PECVD etch in O_2	0.1	1.20 M Ω	20.28%

After comparing the values of Table 4.11 or 4.12 with Table 4.13, we could see that the results were in accordance with the values obtained after simulating the model to calculate the device resistance with different thicknesses of a-C layer. The a-C layer thickness of the as prepared samples (rm_a_01 and rm_a_210) was measured through cross sectional imaging of S-900. It was roughly found to be 30 nm and 20 nm for rm_a_01 and rm_a_210 according to Figure 2.9.Thickness less than 10 nm cannot be measured through cross-sectional imaging of S-900.

However, there was a deviation because the layer of a-C was not continuous throughout and exactly it does not cover the entire interpores region as we had assumed in our model.

4.10 Experimental results of all the processes for comparison of the plasma etching techniques.

Table 4.14: Results obtained for all the plasma etching techniques of all the samples.

	Process	**Reference resistance**	**Sensitivity (%S)**	**Size**
Batch rm_a_229	**1) Plasma oxidation in O_2**			
	As prepared	2.82 kΩ	0.263%	1.8cmx1.2cm
	Front plasma oxidized for 30 s	16.81 kΩ	1.56%	
	Back Plasma oxidized for 30 s	1.07 MΩ	9.53%	
Batch rm_a_229	**2)Plasma Oxidation in Ar**			
	As prepared	185.48 Ω	0.65%	1 cm x0.7 cm
	Front plasma oxidized for 30 s	6.42 kΩ	2.13%	
	Back plasma oxidized for 30 s	94.08 kΩ	8.57%	
	Front plasma oxidized for 30 s	0.54 MΩ	8.95%	
rm_a_210	**3) PECVD process**			
	As prepared	0.57 kΩ	8.35 %	1.3cmx0.8cm
	PECVD for 30 s in O_2	66.61 kΩ	20.28 %	

Table 4.14 continued from previous page:

	4) Water plasma			
	As prepared	1.112kΩ	0.226%	1cm x 0.5cm
	Water plasma 30 s front	75.45 kΩ	6.57%	
	Water plasma 30 s back	0.98 MΩ	9.08%	
rm_a_01	**PECVD in O_2**			
	As prepared	0.89 kΩ	0.26%	1.2cmx0.7cm
	PECVD front 30 s	57.12 kΩ	9.72%	
	PECVD back 30 s	0.58 MΩ	15.54%	
rm_a_02	**Water plasma**			1 cm x 0.6 cm
Cycling data	As prepared	4.38 kΩ	0.71%	
	Water Plasma 30 s front	21.96 kΩ	15.84 %	
	Water plasma 30 s back	1 MΩ	20.23%	
	Water Plasma 10 s front	1.3 MΩ	22.14%	
rm_a_03	**PECVD in O_2**			0.1cmx0.8cm
Cycling data	As prepared	3.93 kΩ	0.39%	
	PECVD front 30 s	43.66 kΩ	19.36%	
	PECVD back 30 s	1.24 MΩ	22.56%	
	PECVD front 10 s	1.55 MΩ	23.67%	

The results as detailed in Table 4.14 obtained for all the various plasma etching techniques showed that PECVD in oxygen and water plasma gave the highest sensitivity because they were very effective in removing the a-C layer because they were performed in capacitive coupled plasma and at a controlled intensity in pristine and clean environment in vacuum chamber at low pressure and high vacuum whereas the intensity

in microwave plasma oxidation could be controlled by setting the power of microwave but the process was not done in pristine conditions as that of PECVD etch . Plasma oxidation in oxygen was more effective than that in argon gas because the a-C layer was fully removed only after plasma etching both sides for 1 minute with the same intensity and conditions. However, the nanotube tips were oxidized and dangling bonds were created due to which more sites were available for analyte adsorption.

Chapter 5

Conclusion and scope of future work:

Vertically aligned MWCNTs were grown in the highly ordered pores of alumina templates through the pyrolysis of xylene without the use of any catalyst. Fabrication of the alumina template using two step anodization was simple and cost effective as it did not require any complicated steps like photolithography. The MWCNTs grown in the templates were investigated as a resistive sensor material. An excellent response to low concentration of 100 ppm of ammonia was observed. The theoretical modeling of the resistive sensor developed [66] was necessary to understand the current path through the equivalent circuit model to obtain the highest sensor response. The design for the device configuration should be such that the current is made to flow through the alternate path by tailoring the thickness of a-C layer. The simulation model obtained for calculating the device resistance matched with the measured values of device resistance. A model to calculate the change of device resistance with respect to the number of gas molecules was also developed in which we calculated the acceptor density of MWCNTs involved and lifetime of the recombination of electrons injected by ammonia molecules with the holes of the p-type MWCNTs semiconductor of the sensor. The values of resistance of CNTs, top and bottom a-C layers were obtained by the simulation model which was in accord with measured experimental values of resistance with least square error of about 10^-3 as shown in Table 2.4.

A comparative study of various plasma etching techniques was done. Also, we used PECVD chamber to perform oxygen and water vapor plasma etching for the first time to decrease the thickness of a-C layer to enhance the sensitivity. We obtained a very high

cumulative sensitivity of 23 %.We were the first group to develop a sensor which has embedded MWCNTs in the pores of AAO template and has reached a sensitivity of 11% for steady state, 20 % for the first pulse of ammonia and cumulative of about 23% which was almost as good as SWCNT-PABs composite sensor which gave 22% cumulative change of sensitivity to 100 ppm ammonia [59]. All the sensing measurements were done at room temperature and relative humidity of about less than 10 %.

Highest sensitivity of 23% to 100 ppm ammonia was recorded after PECVD etch in oxygen at a flow rate of 20 sccm and RF power tuned at 75 W which was very effective in removing the a-C layer because of the plasma obtained in the highly clean and pristine environment of the vacuum chamber. Water plasma etch was used to remove the a-C layer and open the ends of CNTs in order to enhance the sensitivity. It was also as effective as PECVD etch in oxygen in removing the a-C layer. The PECVD apparatus was used to etch off the a-C layer by the oxygen and water vapor plasma formed at a controlled flow rate of the gas at 20 sccm. This was done at a low base pressure of few milli Torr, and in a clean and high vacuum environment. However, these CNTs do also get functionalized with oxygen groups in this plasma etching process which changes the binding energy at the tips of the CNTs which is responsible for giving a better response to ammonia molecules.

Removing the a-C layer fully and then replacing it with a more conductive layer like metal nanocluster can be expected to give a better response and enhance the sensitivity of the sensor which was observed in the results of metal sputtering experiments. Both the metals Ni and Ti formed ohmic contacts with the CNT layer , which behaved as a p-type semiconductor layer. Sensitivities to 100 ppm ammonia recorded after Ti and Ni

deposition of 3 nm on the back side of the template were 18 % and 23 % respectively as shown in Figure 4.12. This experiment also helped in understanding the current flow path of the model and its relation to the sensitivity of the device. The current flow path optimization of the model was necessary to get the highest sensor response. This was accomplished by making the current choose the alternate path through the MWCNTs. To achieve this, we made the direct current path too resistive by decreasing the a-C layer thickness. Note that the thickness of a-C layer is inversely proportional to resistance of the top and bottom layers of a-C.

Many other plasma etching techniques in various atmospheres like water plasma or argon can be studied in detail. Detailed study can be done on plasma etching techniques of how the sensor binding energy and work function are changed with respect to the removal of a-C layer. This would also help us to find out new techniques to remove the a-C layer. Also, functionalization of the CNTs with metal nanoclusters is underway to improve the sensitivity and develop a better sensor.

Appendix

Appendix A

```
 %Calculating Rdevice of AAO CNT template
%Written by Shripriya Poduri(shripriya@uky.edu)
%Date :May 2010
ro=input('Enter the pore radius')
L1=input('enter the pore pitch in x and y directions')
rhoac=input('Enter the resistivity of amorphous carbon')
rhocnt=input('Enter the resistivity of carbon nanotube')
hcnt=input('Enter the height of CNTs')
do=input('Enter the outer diameter')
di=input('Enter the inner diameter')
tactop=input('Enter the top thickness of amorphous carbon')
tacbot=input('Enter the bottom thickness of amorphous carbon')
X=0:pi/100:pi/2    % Generate numbers of interval of pi/100 between 0 to pi/2
Y=roxsin(X)./((L1/2)-ro.xsin(X))
Z=trapz(X,Y)       % Integrating of the area from 0 to pi/2
R1=(rhoac/tactop)x(Z+2x((L1/2-ro)/(L1))) % Equation 2.7 to calculate Rtop
R3=(rhoac/tacbot)x(Z+2x((L1/2-ro)/(L1))) % Equation 2.7 to calculate Rbot
R2=rhocntxhcnt/(pix(do^2-di^2)/4)        % Equation 2.9 to calculate Rcnt
Nx=input('Enter the number of rows of MWCNTs in x direction')
Ny=input('Enter the number of rows of MWCNTs in y direction')
R0i=0
R1i=0
```

```
R2i=0

R2nd=0

R3rd=0

for i=1:Nx    % for loop for summation of resistances after succesive delta to wye
transfomation

   R0i=R0i+(R1x(R2+R3)/(R1+2xR2+R3))

   R1i=R1i+((R1xR2)/(R1+2xR2+R3))

   R2i=R2i+((R2x(R2+R3))/(R1+2xR2+R3))

   if i==2

      R2nd=R2nd+((R1+R1i)x(R3+R2i))/(R1+R2+R3+R1i+R2i)

      R3rd=R3rd+((R1+R1i)x(R2+R3+R2i))/(R1+R2+R3+R1i+R2i)

   end

i=i+1

end

Rrow=R0i+R2nd+R3rd            % Calculating Row resistance

Rd=Nyx(1/Rrow)

Rdevice=1/Rd                  % Rdevice using equation 2.6
```

Appendix B

Program to calculate Device Resistance for a range of thicknesses of a-C layer

```
%Calculating Rdevice of AAO CNT template

%Written by Shripriya Poduri(shripriya@uky.edu)

%Date :May 2010

ro=input('Enter the pore radius')
```

```
L1=input('enter the pore pitch in x and y directions')

rhoac=input('Enter the resistivity of amorphous carbon')

rhocnt=input('Enter the resistivity of carbon nanotube')

hcnt=input('Enter the height of CNTs')

do=input('Enter the outer diameter')

di=input('Enter the inner diameter')

tactop=0:1x10^-9:40x10^-9    % Range of top a-C layer thickness from 0 to 40 nm

tacbot=0:1x10^-9:40x10^-9   %  Range of bottom layer thickness from 0 to 40 nm

X=0:pi/100:pi/2

Y=roxsin(X)./((L1/2)-ro.xsin(X))

Z=trapz(X,Y)

R1=(rhoac./tactop)x(Z+2x((L1/2-ro)/(L1)))

R3=(rhoac./tacbot)x(Z+2x((L1/2-ro)/(L1)))

R2=rhocntxhcnt/(pix(do^2-di^2)/4)

Nx=input('Enter the number of rows of MWCNTs in x direction')

Ny=input('Enter the number of rows of MWCNTs in y direction')

R0i=0

R1i=0

R2i=0

R2nd=0

R3rd=0

for i=1:Nx

   R0i=R0i+(R1.x(R2+R3)./(R1+2xR2+R3));
```

```
    R1i=R1i+((R1.xR2)./(R1+2xR2+R3))
    R2i=R2i+((R2.x(R2+R3)).(R1+2xR2+R3))
    if i==2
        R2nd=R2nd+((R1+R1i).x(R3+R2i)).(R1+R2+R3+R1i+R2i)
        R3rd=R3rd+((R1+R1i).x(R2+R3+R2i)).(R1+R2+R3+R1i+R2i)
    end
i=i+1
end
Rrow=R0i+R2nd+R3rd
Rd=Ny.x(1./Rrow)
Rdevice=1./Rd
```

This program was helpful in calculating the least square error. The calculated device resistance was matched with the measured device resistance to obtain the least square error which was discussed in table 2.3.

References

[1] Iijima S 1991 Nature pp. 354, vol 56, 1991.

[2] W. A. de Heer, A. Chatelain, and D. Ugarte, "A carbon nanotube fieldemission electron source," *Science*, vol. 270, pp. 1179–1180, 1995.

[3] R. H. Baughman, C. Cui, A. A. Zakhidov, Z. Iqbal, J. N. Barasci, G. M. Spinks, G. G. Wallace, A. Mazzoldi, D. de Rossi, A. G. Rinzler, O. Jaschinski, S. Roth, and M. Kertesz, "Carbon nanotube actuators," *Science*, vol. 284, pp. 1340–1342, 1999.

[4] J. Kong, N. R. Franklin, C. Zhou, M. G. Chapline, S. Peng, K. Cho, and H. Dai, "Nanotube molecular wires as chemical sensors," *Science*, vol. 287, pp. 622–625, 2000.

[5] T. Rueckes, K. Kim, E. Joselevich, G. Y. Tseng, C. Cheung, and C. M. Lieber, "Carbon nanotube-based nonvolatile random access memory for molecular computing," *Science*, vol. 289, pp. 94–97, 2000.

[6] J. W. Erisman, R. Otjes, A. Hensen, P. Jongejan, P. van den Bulk, A. Khlystov, H. Mols, and S. Slanina, "Instrument development and application in studies and monitoring of ambient Ammonia," *Atmos. Environ.*, vol. 35, pp. 1913–1922, 2001.

[7] A. Modi, N. Koratkar, E. Lass, B.Q.Wei, P.M. Ajayan, "Miniaturized gas ionization sensors using carbon nanotube", Nature 424 (6945) (2003) 171–174.

[8] J.Y. Chung, K.H. Lee, J. Lee, D. Troya, G.C. Schatz, "Multi-walled carbon nanotube experiencing electrical breakdown as gas sensors", Nanotechnology 15 (11) (2004) 1596–1602.

[9] T. Someya, J. Small, P. Kim, C. Nuckolls, J.T. Yardley, "Alcohol vapor sensors based on single-walled carbon nanotube field effect transistors",Nano Lett. 3 (7) (2003) 877–881.

[10] L. Valentini, C. Cantalini, I. Armentano, J.M. Kenny, L. Lozzi, S. Santucci, "Highly

sensitive and selective sensors based on carbon nanotube thin films for molecular detection", Diamond Relat. Mater. 13 (4–8) (2004) 1301–1305.

[11] H.Y. Jung, S.M. Jung, J.S. Suh, "Chemical sensors for sensing gas adsorbed on the inner surface of carbon nanotube channels", Appl. Phys. Lett. 90 (2007) 153114–153116.

[12] Qin S J, Wu Z J, Tang Z Y, Song Y L, Zeng F Z and Zhao D 2000 *Sensors Actuators* B 66 240

[13] Starke T K H, Coles G S V and Ferkel H 2002 *Sensors Actuators* B 85 239

[14] Bai H and Shi G 2007 *Sensors* **7** 267

[15] Sharma R K, Bhatnagar M C and Sharma G L 1998 *SensorsActuators* B 46 194

[16]P.L. Dickrella, S.K. Pal, G.R. Bournea, C. Muratore, A.A. Voevodin, P.M. Ajayan, L.S. Schadler and W.G. Sawyer Tribology Letters, Vol. 24, No. 1, October 2006

[17] Bekyarova, E.; Davis, M.; Burch, T.; Itkis, M. E.; Zhao, B.; Sunshine, S. and Haddon, R.C.; 2004 *J. Phys. Chem. B* 108, 19717

[18] Kong, Kong, J., Franklin, N., Zhou, C.,Chapline M., Peng S., Cho K., Dai H., 2000 *Science*, 287 622

[19] Suresh Rajaputra, Raghu Mangu, Patricia Clore, Dali Qian, Rodney Andrews and Vijay P. Singh, "Multiwalled carbon nanotube arrays for gas sensing applications" Nanotechnology, v 19, n, 34, August 27 , 2008

[20] Suresh Rajaputra, Raghu Mangu, Ning Ma, Patricia Clore, Dali Qian, Rodney Andrews, Sovannary Phok, Janet Lumpp, and Vijay Singh, "Vertically Aligned Carbon Nanotube Arrays for Room Temperature Gas Sensors" *Nanotube and Related Nanostructures*, edited by Yoke Khin Yap (Mater. Res. Soc. Symp. Proc. Volume 1057E, Warrendale, PA, 2007), 1057-II20-08

[21] Kong, Kong, J., Franklin, N., Zhou, C.,Chapline M., Peng S., Cho K., Dai H., 2000 *Science*, 287 622

[22] J. Sarkar, G. G. Khan, and A. Basumallick, Bull. Mater. Sci. 30 (3), 271-290 (2007).

[23] C. Kumar (editor), Nanomaterials for Biosensors, Wiley-VCH: Weinheim (2007).

[24] A. L. Friedman and L. Menon. J. Elec. Soc. 154 (4), E68-E70 (2007).

[25] L. Menon, Chapter 4: "Synthesis of nanowires in porous alumina." In Quantum Dots and Nanowires, S. Bandyopadhyay and H. Nalwa (editors), American Scientific Publishers: Stevens Ranch, California (2003); pg. 142-191.

[26] Badyopadhyay, Supriyo, "Chapter 3-Electrochemical self-assembly of ordered quantum dots and wire array." In Handbook of nanophase and nanostructured materials, Z. L. Wang Y Lu, and Z. Zhang (editors), Kluwer Academic /Plenum: New York (2003), pg. 121-149.

[27] S. A. Knaack, M. Redden and M. Onellion, "AAO nanopore arrays: A practical entrée to nanostructures", American Journal of Physics, 72 (7), p856-859 (2004).

[28] Eftekhari, A.; Jafarkhani, P; Moztarzadeh, F (2006). "High-yield synthesis of carbon nanotube using a water-soluble catalyst support in catalytic chemical vapor deposition". *Carbon* 44: 1343. doi:10.1016/j.carbon.2005.12.006

[29] Singh, R. Pantarotto, D.; Lacerda, L.; Pastorin, G.; Klumpp, C.; Prato, M.; Bianco, A.; Kostarelos, K. "Tissue biodistribution and blood clearance rates of intravenously administered carbon nanotube radiotracers" *Proc. Natl. Acad. Sci. USA*, vol 103, pp 3357-62, 2006.

[30] I. Sayagoa, H. Santosa, M.C. Horrillo a, M. Aleixandrea, M.J. Fernándeza, E. Terradob, I. Tacchinib, R. Arozc,W.K. Maserb, A.M. Benitob, M.T. Martínezb, J.

Gutiérreza, E. Mu˜nozb, 2008 Elsevier Talanta 77 (2008) 758–764

[31] Snow E S, Perkins F K and Robinson J A 2006 *Chem. Soc. Rev.* 35 790

[32] http://www.engr.uky.edu/~cense/equipment/plasmaetch.html

[33] P.L. Dickrella, S.K. Pal, G.R. Bournea, C. Muratore, A.A. Voevodin, P.M. Ajayan, L.S. Schadler and W.G. Sawyer Tribology Letters, Vol. 24, No. 1, October 2006

[34] Benoit Ruelle, Alexandre Felten, Jacques Ghijsen, Wolfgang Drube,Robert L Johnson5, Duoduo Liang6, Rolf Erni6, Gustaaf Van Tendeloo,Philippe Dubois, Michel Hecq and Carla Bittencourt, J. Phys. D: Appl. Phys. 41 (2008) 045202

[35] Changlun Chen, Bo Liang, Akihisa Ogino, Xiangke Wang, and Masaaki Nagatsu,J. Phys. Chem. C 2009**,** 113, 7659–7665

[36] Martin S. Bell, Kenneth B. K. Teo, Rodrigo G. Lacerda1, W. I. Milne, David B. Hash, and M. Meyyappan *Pure Appl. Chem.*, Vol. 78, No. 6, pp. 1117–1125, 2006.

[37] Seong Chu Lim, Chul Su Jo, Hee Jin Jeong, Young Min Shin, Young Hee Lee, Iran Amildo Samayoa and Jaewu Choi, Jpn. J. Appl. Phys. Vol. 41 (2002) pp. 5635–5639

[38] Bekyarova, E.; Davis, M.; Burch, T.; Itkis, M. E.; Zhao, B.; Sunshine, S. and Haddon, R.C.; 2004 *J. Phys. Chem. B* 108, 19717

[39] Singh, R. Pantarotto, D.; Lacerda, L.; Pastorin, G.; Klumpp, C.; Prato, M.; Bianco, A.; Kostarelos, K. “Tissue biodistribution and blood clearance rates of intravenously administered carbon nanotube radiotracers” *Proc. Natl. Acad. Sci. USA*, vol 103, pp 3357-62, 2006.

[40] Changlun Chen, Akihisa Ogino, Xiangke Wang, and Masaaki Nagatsu Appl. Phys. Lett. 96, 131504 (2010); doi:10.1063/1.3377007

[41] Shaoming Huang and Liming Dai, JPhys. Chem B 2002,106, 3543-3545

[42] Changlun Chen, Bo Liang, Akihisa Ogino, Xiangke Wang, and Masaaki Nagatsu,J. Phys. Chem. C 2009**,** 113, 7659–7665

[43] W. Chen, D. Liming, R. Ajit and T. Tia Benson, *J. Am. Chem. Soc.* 128 (2006), p. 1412.

[44] V.P. Singh, A. Aguilera, V. Jayaraman, S. Sanagapalli, R.S. Singh, V. Jayaraman and K. Sampson, *Sol. Energy Mater. Sol. Cells* 90 (2006), pp. 713–726.

[45] http://rsbweb.nih.gov/ij/

[46] Stransfield, Alfred. The Electric Furnace: Its Construction, Operation and Uses. New York: McGraw-Hill, 1914.

[47] Rothwell, Richard Pennefather. The Mineral Industry. New York: Scientific Publishing, 1903

[48] Fink, Donald G., and H. Wayne Beaty. Standard Handbook for Electrical Engineers. 11th. New York: McGraw-Hill, 1978.

[49] Serway, Raymond A., and Jerry S. Faugh.*College Physics. 6th Edition*. Belmont, CA: Thomson, 2003

[50] Carbon, Vol. 33, No. 7, pp. 941-948. 1995 Copyright 0 1995 Elsevier Science Ltd J.-P. ISSI,' L. LANGER,' J. HEREMANS,and C. H. OLK.

[51] A. Yu. Kasumov, I. I. Khodos, P. M. Ajayan and C. Colliex, *Europhys. Lett.*, 34 (6), pp. 429-434 (1996)

[52] Quoc Ngo, Petranovic, S.Krishnan, Alan Cassell, IEEE transactions on Nanotechnology Vol 3 No. 2 June 2004.

[53] Snow E S, Perkins F K and Robinson J A 2006 *Chem. Soc. Rev.*35 790

[54] P.L. Dickrella, S.K. Pal, G.R. Bournea, C. Muratore, A.A. Voevodin, P.M. Ajayan,

L.S. Schadler and W.G. Sawyer Tribology Letters, Vol. 24, No. 1, October 2006

[55] Benoit Ruelle, Alexandre Felten, Jacques Ghijsen, Wolfgang Drube,Robert L Johnson5, Duoduo Liang6, Rolf Erni6, Gustaaf Van Tendeloo,Philippe Dubois, Michel Hecq and Carla Bittencourt, J. Phys. D: Appl. Phys. 41 (2008) 045202

[56] Changlun Chen, Bo Liang, Akihisa Ogino, Xiangke Wang, and Masaaki Nagatsu,J. Phys. Chem. C 2009**,** 113, 7659–7665

[57] Martin S. Bell, Kenneth B. K. Teo, Rodrigo G. Lacerda1, W. I. Milne, David B. Hash, and M. Meyyappan *Pure Appl. Chem.*, Vol. 78, No. 6, pp. 1117–1125, 2006.

[58] Seong Chu Lim, Chul Su Jo, Hee Jin Jeong, Young Min Shin, Young Hee Lee, Iran Amildo Samayoa and Jaewu Choi, Jpn. J. Appl. Phys. Vol. 41 (2002) pp. 5635–5639

[59] Bekyarova, E.; Davis, M.; Burch, T.; Itkis, M. E.; Zhao, B.; Sunshine, S. and Haddon, R.C.; 2004 *J. Phys. Chem. B* 108, 19717

[60] Suresh Rajaputra, Raghu Mangu, Patricia Clore, Dali Qian, Rodney Andrews and Vijay P. Singh, "Multiwalled carbon nanotube arrays for gas sensing applications" Submitted to Nanotechnology (2008), 19 March 2010, 19 (2008) 345502

[61] Azad Naeemi, *Senior Member, IEEE*, and James D. Meindl, Life Fellow, IEEE, IEEE electron device letters, Vol. 27, no. 5, May 2006,340

[62] A. Yu. Kasumov, I. I. Khodos, P. M. Ajayan and C. Colliex, Europhys. Lett. 34 (6), pp. 429-434 (1996) ,430

[63] Kai Xiao, Yunqi Liu, Ping'an Hu, Gui Yu, Yanming Sun, and Daoben Zhu J. AM. CHEM. SOC. 2005, 127, 8614-8617

[64] Robert V. Seidel, Andrew P. Graham, Georg S. Duesberg, Maik Liebau, Eugen Unger, Franz Kreupl, Wolfgang Hoenlein 12th GAAS Syposium Amsterdam 2004

[65] Feng wang, Gordana Dukovic, Louis E. Brus and Tony F Heinz ,PhysRevLetter 92.177401.

[66] Raghu Mangu, Suresh Rajaputra, Patricia Clore, Dali Qian, Rodney Andrews and Vijay P. Singh, Materials Science and Engineering: B, 19 March 2010, 19 (2008) 345502

[67] Masashi Shiraishi, Koichiro Hinokuma and Masafumi Ata , 2000 American Institute of Physics 1-56396-973-4/007

[68] Peng Liu, Yang Wei, Kaili Jiang, Qin Sun, Xiaobo Zhang, and Shoushan Fan, PHYSICAL REVIEW B **73**, 235412 _2006

[69**]** Hiroki Ago,Thomas Kugler, Franco Cacialli, William R. Salaneck, Milo S. P. Shaffer,Alan H. Windle, and Richard H. Friend, *J. Phys. Chem. B* 1999, *103,* 8116-8121

[70] Patricia A Clore Thesis, University of Kentucky, 2008,6-11

[71] http://en.wikipedia.org/wiki/Titanium

[72] http://en.wikipedia.org/wiki/Nickel

[73] Raghu Mangu Thesis,University of Kentucky, December 2008,56

Vita

Shripriya Poduri was born on April 8, 1986 in Kakinada, India. She did her Bachelor of Engineering in Electronics, Electrical & Communication (EECE) from Panjab University, India from 2004-2008. During her undergraduate studies, she did her research internship in Microelectronics Division under the guidance of Scientist F level, Dr. C Ghanshyam in Central Scientific Instrumentation Organization (CSIO), Chandigarh, India. There, she developed gas monitoring System for environmental toxic gases using Metal Oxide Sensors and assisted in research. Furthermore, she served as an intern in Semiconductor Complex Ltd, Mohali in India and was trained in VLSI.